Received: 21 November 2023 | Revised: 4 May 2024 | Accepted: 12 June 2024

DOI: 10.1002/qj.4816

Quarterly Journal of the Royal Meteorological Society RMetS

RESEARCH ARTICLE

Summer Heatwaves in Southeastern Australia

Cameron R. Henderson[1,2] | **Michael J. Reeder**[2,3] | **Teresa J. Parker**[2,3,4] | **Julian F. Quinting**[2,3,5] | **Christian Jakob**[2,3,6]

[1]Bureau of Meteorology Training Centre, Broadmeadows, Victoria, Australia

[2]School of Earth, Atmosphere and Environment, Monash University, Clayton, Victoria, Australia

[3]Australian Research Council Centre of Excellence for Climate Extremes, Monash University, Clayton, Victoria, Australia

[4]Environment, Commonwealth Scientific and Industrial Research Organisation, Hobart, Australia

[5]Institute of Meteorology and Climate Research Troposphere Research (IMK-TRO), Karlsruhe Institute of Technology, Karlsruhe, Germany

[6]Australian Research Council Centre of Excellence for the Weather of the 21st Century, Monash University, Clayton, Victoria Australia

Correspondence
Cameron R. Henderson, School of Earth, Atmosphere and Environment, Monash University, Building 28, 9 Rainforest Walk, Clayton Campus, Clayton, Victoria, 3800, Australia.
Email: cameron.henderson@monash.edu

Funding information
Australian Research Council, Grant/Award Number: CE170100023; Australian Research Council, CE230100012; Helmholtz Association, Young Investigator Group (SPREADOUT), Grant/Award Number: VH-NG-1243

Abstract

Heatwaves in southeastern Australia have characteristic weather patterns that are well understood but are outnumbered by days with similar synoptic-scale patterns that are not heatwaves. Accordingly, the aim of this study is to identify the key differences between heatwave and non-heatwave days from 40 years of reanalysis data. A synoptic climatology of seven weather states was constructed by *k*-means cluster analysis. Four of these states account for more than 80% of heatwave days across south-and-central eastern Australia. Moreover, the spatial maxima in the frequency of the heatwave days are distinct and geographically separated. Heatwave days have a stronger upper anticyclone or ridge that has propagated further equatorward in comparison with non-heatwave days. The air upstream of the ridge is more humid on heatwave days, whereas downstream of the ridge the air is much drier. These dry anomalies are co-located with midtropospheric subsidence and the moist anomalies with ascent, and their respective spatial distributions are consistent with regions of adiabatic warming and latent heating identified in recent studies of southeast Australian heatwaves. The corresponding vertical motion on non-heatwave days is weaker and shifted further poleward. Southeast Queensland heatwave days exhibit increased baroclinicity over the Australian Subtropics and reduced rainfall over Queensland. Further south and west, heatwave days are associated with more amplified Rossby waves and increased rainfall over the Australian Tropics. Anticyclonic Rossby wave breaking is greatly enhanced on heatwave days south of 30°S. For every day in each of these four weather states, the 3-day-mean maximum temperature in the region of peak heatwave day frequency is positively correlated with 500 hPa geopotential height anomalies on the equatorward flank of the cluster-mean upper ridge. These findings underline the importance of equatorward Rossby wave propagation in the dynamics of southeast Australian heatwaves.

KEYWORDS

cluster analysis, dynamics, heatwaves, southeastern Australia

1 | INTRODUCTION

Heatwaves cause more excess fatalities in Australia than any other natural hazard (Coates *et al.*, 2014, 2022). They are similarly deadly in other parts of the world (Barriopedro *et al.*, 2011; Robine *et al.*, 2008). In southeastern Australia, the heatwave that began in late January 2009 was the longest and hottest on instrumental record for many locations (National Climate Centre, 2009) and culminated in the devastating bushfires of Black Saturday on February 7, 2009, in the state of Victoria (Engel *et al.*, 2013). With the assessment that heatwaves will very likely become more frequent in a warming climate (IPCC, 2007), a major research effort ensued to better understand the meteorology of Australian heatwaves, especially those affecting densely populated southeastern Australia (Figure 1). For Australia, a heatwave at a specified location is often defined as a period of three or more consecutive days on which the maximum temperature exceeds the 90th percentile for the time of year (Perkins & Alexander, 2013). Definitions with additional criteria based on the minimum temperature and an excess heat factor (Nairn *et al.*, 2009) are also common.

A consistent finding of this research is that heatwaves in southeastern Australia are associated with anticyclonic upper tropospheric anomalies (Parker *et al.*, 2013, 2014; Pezza *et al.*, 2012; Purich *et al.*, 2014; Quinting & Reeder, 2017; Risbey *et al.*, 2017). These anomalies are typically strongest in heatwaves affecting the southern states of Victoria and Tasmania and decrease in strength over subtropical regions, including central-eastern New South Wales (Parker *et al.*, 2019) and southeastern Queensland (Quinting *et al.*, 2018). Similar findings regarding the role of anticyclones in heatwaves have been reported elsewhere in the world (Black *et al.*, 2004; Galarneau *et al.*, 2012; Matsueda, 2011; Schumacher *et al.*, 2022).

Heatwaves in the state of Victoria are preceded by a Rossby wave train from the southern Indian Ocean (Parker *et al.*, 2014). Near the onset time, an upper tropospheric anticyclonic anomaly amplifies over southeastern Australia, and a surface high-pressure system develops in the Tasman Sea. Composites of the dynamic tropopause for these heatwaves (O'Brien & Reeder, 2017; Parker *et al.*, 2013, 2014; Quinting & Reeder, 2017) have the signature of anticyclonic Rossby wave breaking (Berrisford *et al.*, 2007; Peters & Waugh, 1996; Thorncroft *et al.*, 1993).

Frequent anticyclonic wave breaking over southeastern Australia during the austral summer (Ndarana & Waugh, 2011; Reeder *et al.*, 2015; Song *et al.*, 2011) results from the region's equatorward proximity to the seasonal-mean exit of the midlatitude jet, and also the absence of the thermally induced subtropical jet over Australia at this time of year. The Rossby waveguide is weakened in the jet exit (Hoskins & Ambrizzi, 1993) and Rossby waves are refracted equatorward towards a critical latitude in the Tropics over northern Australia (O'Brien & Reeder, 2017). In their study of heatwaves across four different regions of Australia, Risbey *et al.* (2017) showed that stationary Rossby waves (Takaya & Nakamura, 2001) propagate equatorward of the waveguide and converge into the anticyclone associated with the heatwave. Propagation equatorward of 30°S is suppressed for Victorian heatwaves (Risbey *et al.*, 2017, their figs. 13 and 17), presumably due to reversal of the meridional potential vorticity (PV) gradient in the strong anticyclone. However, Rossby waves propagate equatorward over Australia deeper into the Tropics in other scenarios, such as prior to northern Australia monsoon bursts (O'Brien & Reeder, 2017, their fig. 1), and in episodes of enhanced convection in the South Pacific convergence zone (van der Wiel *et al.*, 2015).

Moisture and diabatic heating are also thought to play an important role in the development of heatwaves. Tropical cyclones northwest of Australia can amplify the upper anticyclone in Victorian heatwaves by perturbing the upper level midlatitude waveguide prior to heatwave onset (Parker *et al.*, 2013). A substantial fraction of the air comprising these upper anticyclones experiences latent heating in the poleward ascending conveyor belt on its upstream flank a few days earlier (Quinting & Reeder 2017), and much of the near-surface air in Victorian and southeastern Queensland heatwaves experiences sensible heating in the planetary boundary layer a few days prior to arrival (Quinting *et al.*, 2018; Quinting & Reeder, 2017). Röthlisberger and Papritz (2023) demonstrated the importance of diabatic heating in the Lagrangian evolution of near-surface air parcels on the annual hottest days for most subtropical and tropical land masses, including Australia.

In this study, heatwaves in southeastern Australia are compared with non-heatwave days using a synoptic climatology derived from a *k*-means cluster analysis of the 500 hPa geopotential height anomalies. Roughly corresponding to the equivalent barotropic level, this is an appropriate field for establishing a set of commonly occurring weather patterns or states, given the known association of heatwaves with Rossby wave propagation. The synoptic climatology is derived from the European Centre of Medium-range Weather Forecasts (ECMWF) Reanalysis v. 5 (ERA5) (Hersbach *et al.*, 2020) of 40 December–March (DJFM) seasons.

Heatwaves are associated with synoptic-scale weather patterns that, at first glance, are not so different from those on many days that do not produce long-lived extreme heat. For instance, there are many summer days with a high-pressure system located in the Tasman Sea, but the majority of these are not heatwave days in Victoria.

FIGURE 1 States and capital cities of southeastern Australia, and surrounding seas. [Colour figure can be viewed at wileyonlinelibrary.com]

Consequently, the dynamical properties of heatwave days and non-heatwave days are analysed for those weather states in which heatwave days occur most often. The ensemble sensitivity technique (Ancell & Hakim, 2007) is then applied to the 3-day-mean maximum temperature to further explore the relationship between prolonged high temperature and pressure and moisture fields in these weather states.

The data and methods are described in Section 2 and the summer synoptic climatology of southeastern Australia is presented in Section 3. Section 4 compares the mean properties of heatwave days with non-heatwave days, and Section 5 examines the ensemble sensitivity of 3-day-mean maximum temperature to pressure and moisture fields for the same regions. Section 6 contains a summary and conclusions.

2 | DATA AND METHOD

2.1 | Data

Daily surface maximum and minimum temperature from the Australian Water Availability Project (AWAP) 0.05° × 0.05° dataset (Jones *et al.*, 2009) are used to identify heatwaves. All other fields are obtained or computed from ERA5 (0.25° × 0.25°). Most fields are daily data at 00 UTC, although rainfall is an accumulation over the 24 hr prior to 00 UTC. The dataset in this study consists of 40 consecutive extended summers (DJFM) from 1979/1980 to 2018/2019, which is a total of 4,850 days. March is included as the longest recorded run of consecutive days on which the maximum temperature was at least 30°C in Melbourne occurred from March 4 to 12, 2013.[1]

2.2 | Synoptic climatology

The synoptic climatology is derived by a *k*-means cluster analysis (Hartigan & Wong, 1979) of daily 500 hPa geopotential height anomalies over the domain 22°S–54°S and 120°S–170°E (Figure 2h). The anomalies are calculated by subtracting the mean, the first four harmonics, and a linear trend from the 40-year daily time series of geopotential height. The domain is similar to the latitude–longitude range of positive 1,000–500 hPa thickness anomalies associated with Victorian heatwaves (Parker *et al.*, 2014, their fig 1d). Although this technique is not the only choice available, it has been used effectively to group synoptic-scale structures in many studies, including those of heatwaves in southeastern Australia (Parker *et al.*, 2013).

2.3 | Heatwaves

Heatwaves at each grid point are identified using the same method as Parker *et al.* (2014). For a single grid point, each heatwave day is one of a 3-day sequence in which the maximum temperature on each day exceeds the 90th percentile for the time of year, and the minimum temperature on two out of the 3 days is also above the 90th percentile. Calendar month percentiles are used. For a spatial domain enclosing multiple grid points with land area >400,000 km^2, the term "regional heatwave day" (RHW day) is used to describe any

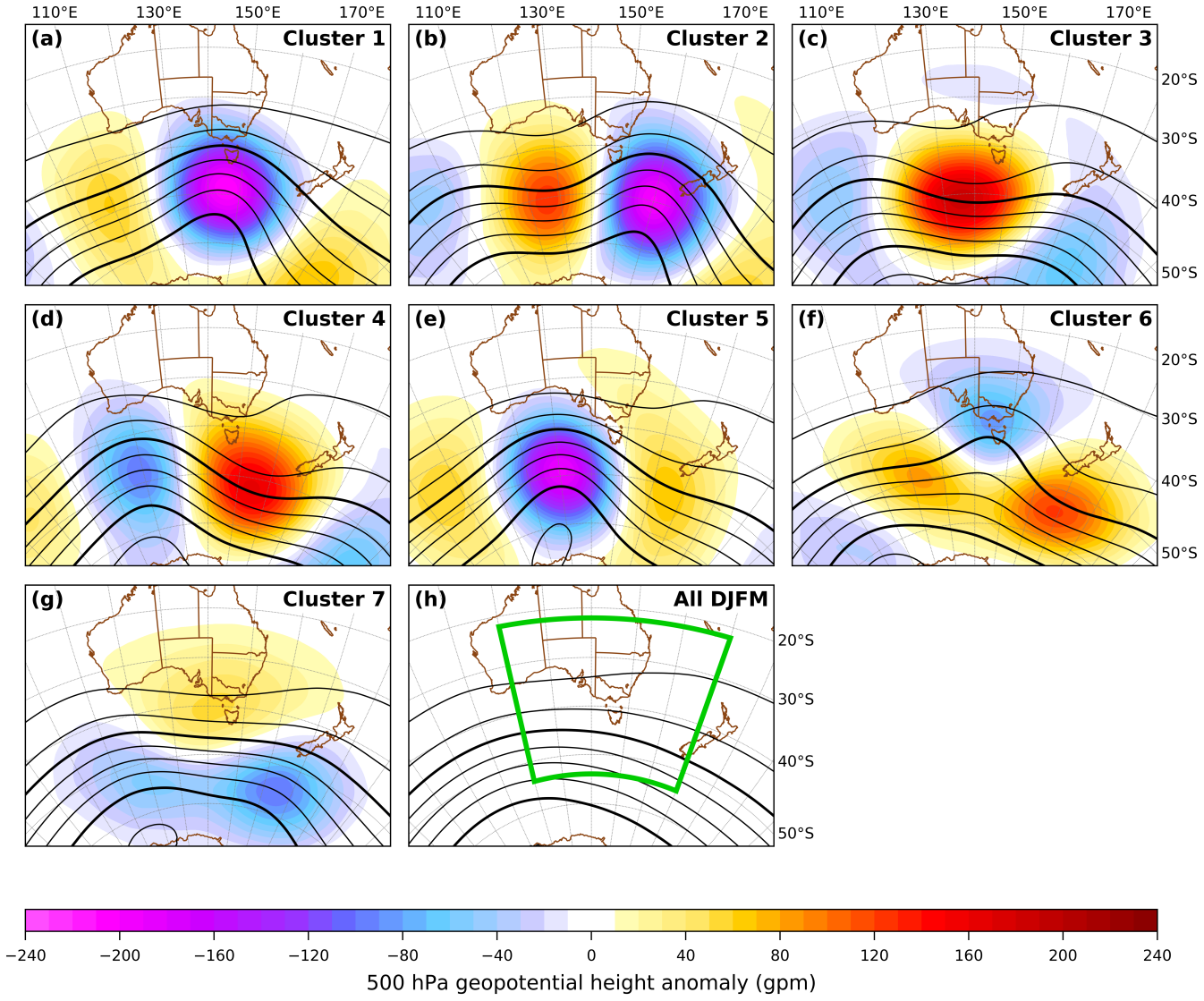

FIGURE 2 (a–g) Cluster centroids of 00 UTC 500 hPa geopotential height anomalies (fill) and corresponding absolute 500 hPa geopotential height (contours). (h) Composite analyses of all December–March (DJFM) days with the cluster analysis domain (green boundary). Contour interval of 100 m with bold contours for $z \leq 5{,}600$ m at intervals of 400 m, decreasing to the south. [Colour figure can be viewed at wileyonlinelibrary.com]

day for which the grid-point heatwave criteria are satisfied over grid points that collectively represent 10% or more of the land area within the domain's boundary, accounting for latitudinal variation. Thus, the RHW day frequency must equal or exceed the maximum heatwave day frequency at any individual point in the chosen domain. Any day on which this 10% of the area threshold is not met is referred to as a "regional non-heatwave day" (NHW day).

2.4 | Statistical testing

The statistical significance of the difference between composite 500 hPa geopotential height anomalies of h RHW days and n NHW days in a single cluster is assessed using a two-sample, two-sided, test of mean. The tests are based on 10,000 random shuffles of the $h + n$ cluster dates into two subsets of size h and n, with a null hypothesis of no difference in mean. Decorrelation times for the anomalies are obtained by modelling the time series at each grid point as an AR(p) process with $1 \leq p \leq 8$, optimised according to the Bayesian information criterion—see Trenberth (1985) or Wilks (2006), Chapter 8. Variance inflation at each grid point due to serial correlation in the anomalies is computed by assuming the first cluster occurrence in each DJFM season is independent, with subsequent cluster occurrences only considered independent if they arise after the decorrelation time has elapsed from the most recent independent cluster occurrence.

2.5 | Rossby wave breaking

A method similar to Song *et al.* (2011) is used to identify Rossby wave breaking on the 350 K isentropic surface and to characterise it as either anticyclonic or cyclonic. The data are initially smoothed to 2.5° × 2.5° resolution using spherical harmonics; and then using Fourier analysis, the zonal wave number is truncated at 15 to filter out sub-synoptic-scale variation. All cut-off anomalies are removed, after which longitude intervals in which the dynamic tropopause (−2 PVU, where 1 PVU is 10^{-6} m^2 ·s^{-1} ·K·kg^{-1}) is crossed more than once when travelling due north from the South Pole to the Equator are identified as wave-breaking features. Wave breaking is then categorised as either anticyclonic or cyclonic based on the sequence of contour turns (anticlockwise, A, or clockwise, C) made by successive longitude extrema on the −2 PVU contour. For instance, the sequence of contour turns AC corresponds to a simple anticyclonic wave-break in the Southern Hemisphere, and CA to a simple cyclonic wave-break.

2.6 | Blocking

Earlier studies have associated blocking anticyclones with Australian heatwaves (e.g., Parker *et al.*, 2014; Risbey *et al.*, 2017) and Northern Hemisphere daily temperature extremes (Pfahl & Wernli, 2012). Here, the blocking is defined using the one-dimensional Tibaldi–Molteni blocking index. The index identifies large, persistent and slow-moving anticyclonic anomalies in the midlatitude 500 hPa geopotential height field as a function of longitude—(refer to Tibaldi *et al.*, 1994, for details). Their latitude window of 3.75° is increased to 5° in this study. Based on the analysis of Schalge *et al.* (2011), a 3-day rather than 5-day persistence criterion is adopted, which reflects the shorter-lived nature of Southern Hemisphere blocking.

3 | SYNOPTIC CLIMATOLOGY

Solutions of the cluster analysis were determined for $k = 2, \ldots, 12$. The use of seven clusters was found to strike the best balance between having clusters of reasonably large size (>10%) and identifying synoptic-scale weather patterns with substantial differences. Following Rossow *et al.* (2005), the latter condition was enforced by requiring the pattern correlations between all clusters to not exceed 0.6. Neither threshold was met when k was increased to 8.

The cluster-mean 500 hPa geopotential height anomalies for $k = 7$ are presented in Figure 2 with the corresponding absolute 500 hPa geopotential height fields. Cluster occurrences and frequencies are given in Table 1. Composite fields of mean-sea-level pressure (MSLP) and 850 hPa temperature for the same cluster dates are shown in Figure 3, together with the grid-point heatwave-day frequency, computed as the ratio of the number of heatwave days at a grid point in the given cluster to the total number of days in that cluster. The characteristics of each cluster are briefly described in the following.

- **Cluster 1: Victoria post-frontal (13.4%)** An upper trough is located south of eastern mainland Australia (Figure 2a) and a cool post-frontal regime extends across Victoria, with the preceding surface trough situated over northeastern New South Wales and central Queensland (Figure 3a). This synoptic pattern has been linked with heatwaves in southeastern Queensland (Gibson *et al.*, 2017; Quinting *et al.*, 2018). A prominent maximum in the grid-point heatwave-day frequency occurs over south and central eastern Queensland.
- **Cluster 2: High in the Bight (12.0%)** An upper ridge is located south of Western Australia (Figure 2b), and a surface high-pressure cell is located in the Great Australian Bight (Figure 3b). Cool air extends over southeastern Australia, with heatwave days occurring preferentially over the southwest of the continent.
- **Cluster 3: Broad High south of eastern Australia (14.4%)** A strong positive 500 hPa geopotential height anomaly south of Australia (Figure 2c) accompanies a broad surface high-pressure system south of eastern Australia (Figure 3c). Although cooler easterly flow occurs over much of New South Wales and southern Queensland, the frequency of heatwave days is slightly above average over western Victoria and southwestern South Australia.
- **Cluster 4: High in the Tasman Sea (16.3%)** An upper ridge in the south Tasman Sea extends northwest over

TABLE 1 Cluster occurrences, frequencies, and domain area-averaged 500 hPa geopotential height root-mean-square (RMS) distance from climatology.

Measurement	Cluster 1	Cluster 2	Cluster 3	Cluster 4	Cluster 5	Cluster 6	Cluster 7	Total
Occurrence (days)	648	582	700	790	792	571	767	4,850
Frequency (%)	13.4	12.0	14.4	16.3	16.3	11.8	15.8	100.0
Mean RMS anomaly (gpm)	73.6	75.3	68.3	60.0	63.1	42.2	31.6	0.00

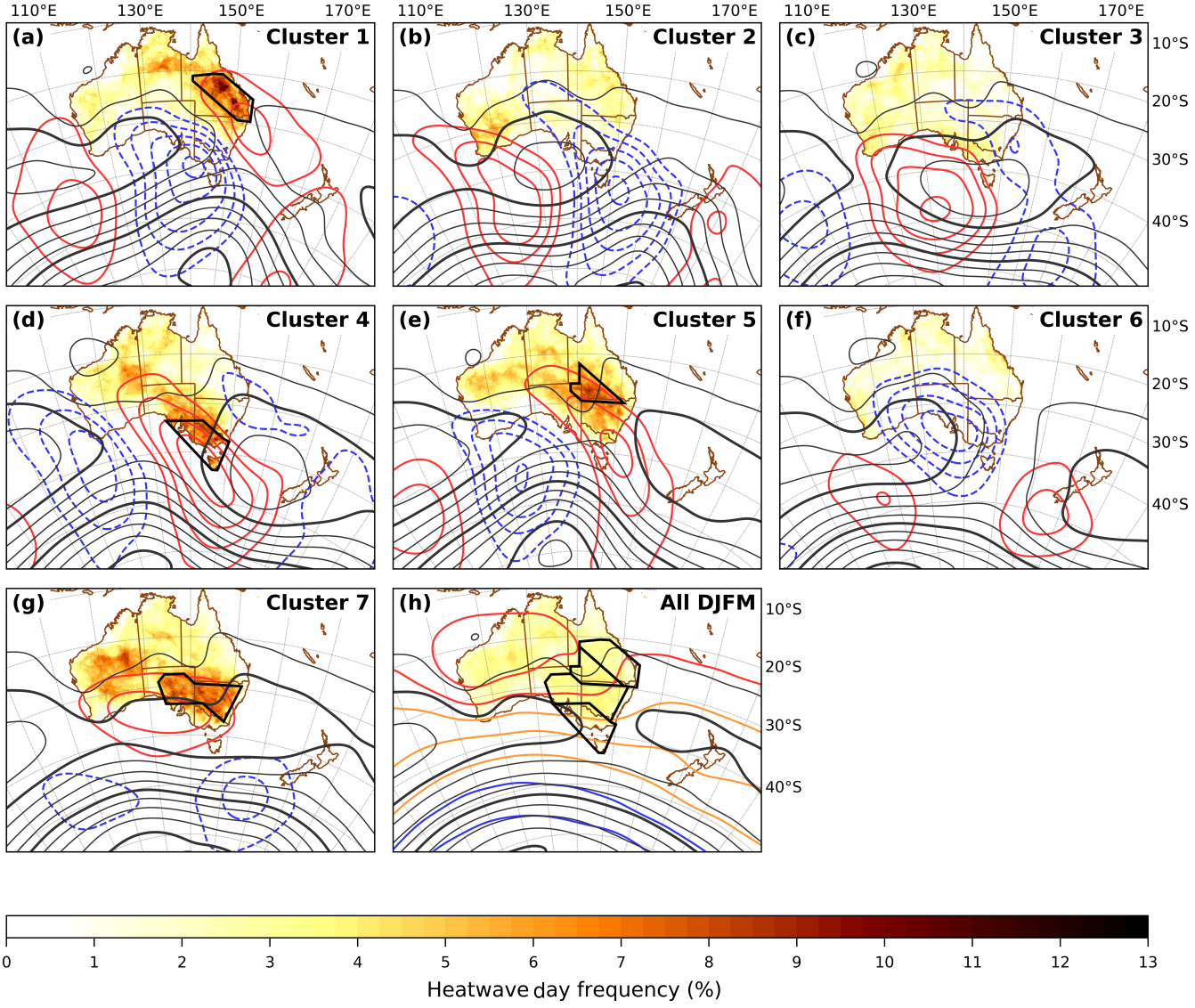

FIGURE 3 (a–g) Mean-sea-level pressure (MSLP; black contours), 850 hPa temperature anomalies (contours, with red positive, blue dashed negative, and zero omitted), and grid-point heatwave-day frequency (fill) for the same cluster dates as Figure 2. MSLP contour interval of 4 hPa with bold contours every 16 hPa for ≤1,016 hPa, decreasing southwards. Contour interval for 850 hPa temperature anomalies is 2°C. (h) MSLP, 850 hPa temperature analyses with 4°C contour interval (northern red contour 20°C) decreasing poleward, and grid-point heatwave-day frequency for all December–March (DJFM) days. Black polygons are the regional heatwave subdomains. [Colour figure can be viewed at wileyonlinelibrary.com]

TABLE 2 Descriptions of subdomains in the four weather states with the largest spatial peaks in the grid-point heatwave-day frequency, and the number (percentage) of regional heatwave days for that subdomain in the corresponding cluster.

Cluster	Weather state	Subdomain with large percentage of heatwave days	Label	RHW days	NHW days
1	Victoria post-frontal	South and central eastern Queensland	SEQ	126 (19.4%)	522 (80.6%)
4	High in the Tasman Sea	Victoria, Tasmania, southeastern South Australia	VIC	122 (15.4%)	668 (84.6%)
5	Victoria pre-frontal	Southwestern Queensland	SWQ	121 (15.3%)	671 (84.7%)
7	Weakly amplified flow	Inland New South Wales, eastern South Australia	NSW	130 (16.9%)	637 (83.1%)

Abbreviations: RHW, regional heatwave; NHW, regional non-heatwave.

southeastern Australia (Figure 2d), and a strong surface high-pressure system is situated in the Tasman Sea with a ridge extending over eastern Queensland (Figure 3d). Temperature at 850 hPa is elevated over Victoria, South Australia, southwestern New South Wales, and Tasmania. The grid-point heatwave-day frequency is the

highest of all the clusters for these regions, and the MSLP field is very similar to the composite pattern associated with Victorian heatwaves (Parker *et al.*, 2014).

- **Cluster 5: Victoria pre-frontal (16.3%)** With a strong trough at 500 hPa south of the Great Australian Bight (Figure 2e), a northeastward temperature gradient at 850 hPa normal to the South Australian coast, and a surface trough over western Victoria (Figure 3e), this pattern contains the ingredients for coastal frontogenesis in southwestern Victoria (e.g., Reeder & Smith, 1987). The maximum frequency in the grid-point heatwave days occurs over southwestern Queensland, northern New South Wales and northeastern South Australia, on the northeastern flank of the heat trough of eastern Australia (Leslie, 1980).
- **Cluster 6: Upper trough over southeastern Australia (11.8%)** An upper trough is located over southeastern Australia (Figure 2f) with a surface pressure trough over the western Tasman Sea (Figure 3f). Cool air extends over Victoria, South Australia, and New South Wales, and heatwave-day frequency over southeastern Australia is the lowest of all the clusters.
- **Cluster 7: Weakly amplified flow (15.8%)** A weak positive 500 hPa geopotential height anomaly extends over southeastern Australia (Figure 2g). The domain area-averaged root-mean-square (RMS) anomaly is the smallest of all the cluster centroids (Table 1) and is less than half the RMS distance from the 500 hPa geopotential height climatology of several other cluster means. This indicates that this cluster is generally comprised of weaker and/or smaller scale anomalies by comparison. The composite MSLP field consists of a weak zonal high-pressure ridge south of the mainland. The temperature at 850 hPa is elevated over most of southern Australia, and a region of peak grid-point heatwave-day frequency occurs through inland New South Wales and central eastern South Australia (Figure 3g).

Four of the weather states—Clusters 1, 4, 5, and 7—account for 82% of all grid-point heatwave days over Australian land south of 20°S and east of 135°E. Each of these weather states show a regionally distinct spatial peak in grid-point heatwave-day frequency. To aid the analysis of the heatwave days in each of these states, and foreshadowing the ensemble sensitivity analysis in Section 5, a subdomain enclosing the region of peak grid-point heatwave-day frequency has been constructed (polygons in Figure 3a,d,e,g). These distinct subsets cover almost all parts of south and central eastern Australia where the grid-point heatwave-day frequency is greater than 3% (Figure 3h). A description and label for the four cluster subdomains is provided in Table 2, along with their frequencies of RHW and NHW days. Table 3 shows the number of days in each cluster that are RHW days over each of the four subdomains, and the percentage of DJFM days that are RHW days (their climatological RHW day frequency). For each subdomain, RHW days occur with highest frequency in the cluster identified in Table 2, at around twice their climatological frequency. Over the Victoria, Tasmania, southeastern South Australia (VIC) subdomain, for example, 122 (41.6%) of its RHW days occur in Cluster 4, on 15.4% of days in that cluster, which is more than two-and-a-half times the VIC climatological RHW day frequency of 6.0%.

In each of Clusters 1, 4, 5, and 7, RHW days represent less than 9% of days in the associated subdomain. Given the synoptic similarity of days belonging to a particular cluster, an examination of the differences between RHW and NHW days in these cluster subdomains is appropriate.

4 | HEATWAVE DAYS VERSUS NON-HEATWAVE DAYS

MSLP and anomalies of 500 hPa geopotential height, precipitable water, and past-24-h precipitation are presented for each of the four cluster subdomains, with composites of RHW days, NHW days, and their difference. The evolutions of these composite events are illustrated with Hovmöller diagrams of the 350 K PV, AWB, 400–600 hPa

TABLE 3 Number of regional heatwave days that fall in each cluster and the total number of regional heatwave days (percentage of December–March [DJFM] days) for each subdomain.

	Number of regional heatwave days							
Region	**Cluster 1**	**Cluster 2**	**Cluster 3**	**Cluster 4**	**Cluster 5**	**Cluster 6**	**Cluster 7**	**All DJFM**
SEQ	126	49	19	28	81	27	49	379 (7.8%)
VIC	2	6	48	122	41	1	73	293 (6.0%)
SWQ	68	36	25	48	121	8	93	399 (8.2%)
NSW	23	20	36	99	107	4	130	419 (8.6%)

Abbreviations: NSW, inland New South Wales, eastern South Australia; SEQ, south and central eastern Queensland; SWQ, southwestern Queensland; VIC, Victoria, Tasmania, southeastern South Australia.

averaged omega vertical velocity, and blocking (3-day Tibaldi–Molteni blocking index), with day 0 corresponding to the composite dates of Figures 2 and 3. For RHW days, these may be loosely interpreted as rolling 3-day averages, but not exactly, as the duration of heatwaves can be greater than 3 days. The anomaly fields of PV, AWB, and omega are averaged over latitudes 24°S–66°S and 7.5° longitude intervals. As the highest frequency of AWB climatologically is in the eastern Pacific in DJFM (e.g., Reeder *et al.*, 2015; Song *et al.*, 2011), the results for this field are divided by the climatological frequency for each longitude interval to emphasise AWB in the Australian region.

4.1 | Cluster 1, SEQ subdomain

An elongated positive 500 hPa geopotential height anomaly lies over the southern Northern Territory and Queensland on RHW days, with an extensive region of mid-tropospheric subsidence over northern Queensland and the Coral Sea on its northeastern flank (Figure 4a). Neither of these features are present on NHW days (Figure 4b). The positive difference in the 500 hPa geopotential height pattern in the vicinity of the upper ridge is statistically significant (Figure 4c), as is the negative difference south of mainland Australia. Together, these imply stronger baroclinicity between 25°S and 45°S at Australian longitudes on RHW days. The surface trough south of mainland Australia and its extension into the heat trough of eastern Australia are deeper on average for RHW days. Precipitation is reduced over Queensland and the Australian Tropics on RHW days (Figure 4d–f) but is enhanced near the South Pacific convergence zone, and precipitable water is below average over a region that closely matches the location of the mid-tropospheric subsidence.

Figure 5 shows the evolution of the pressure and moisture fields for RHW cases at 2-day intervals from day −6 to day −2. A strong spatial correspondence between

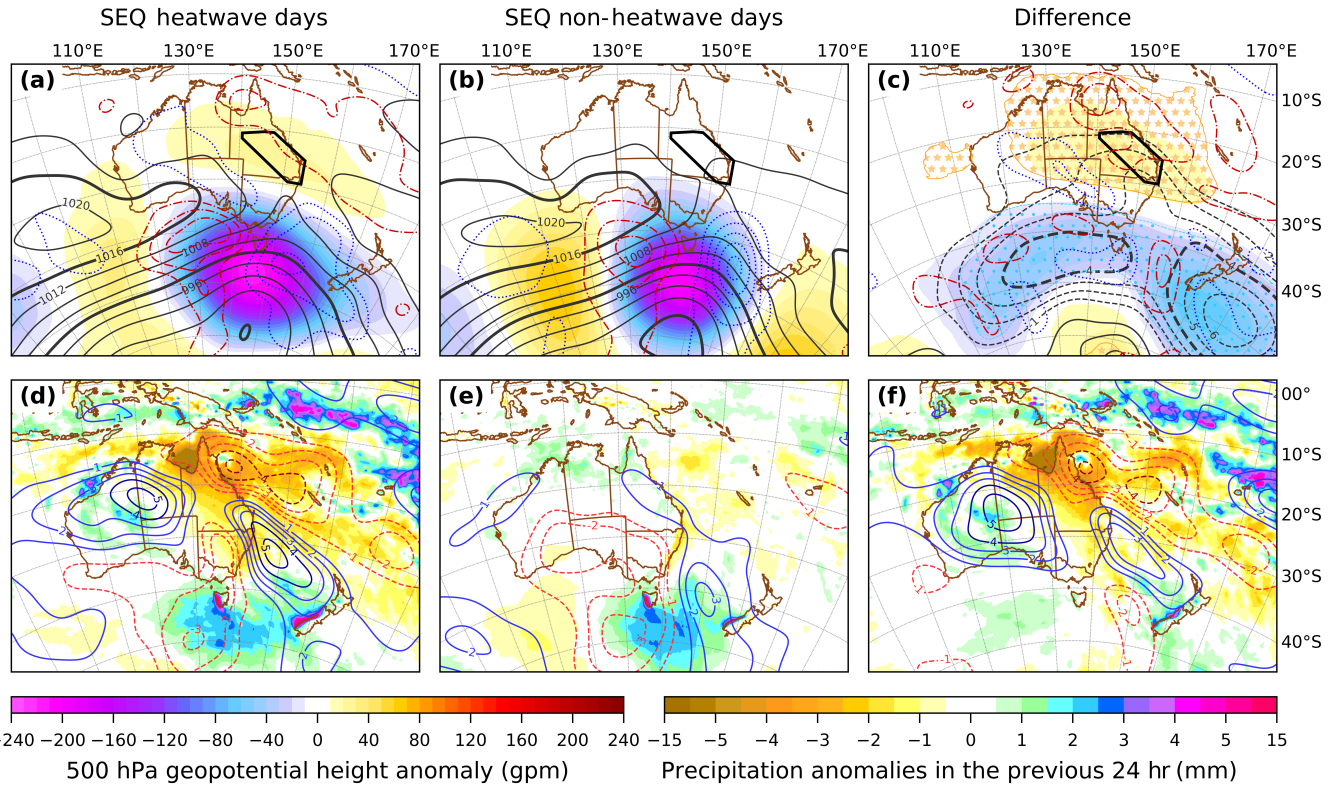

FIGURE 4 (a–c) The 500 hPa geopotential height anomalies (fill), mean-sea-level pressure (MSLP; black contours), and 400–600 hPa averaged omega vertical velocity anomalies (red dash-dot contours positive and blue dotted contours negative) for (a) regional heatwave days and (b) regional non-heatwave days in Cluster 1, south and central eastern Queensland (SEQ) domain (black polygon). MSLP contour intervals are as per Figure 3, and omega anomalies are contoured every 0.02 $Pa \cdot s^{-1}$ with zero omitted. The difference, (a) minus (b), is shown in (c) with these MSLP contours every 1 hPa, negative dashed, zero omitted, and bold every ±4 hPa. Orange star (light blue dot) stippling in (c) shows regions where the regional heatwave-day composite 500 hPa geopotential height anomaly is greater than (less than) its regional non-heatwave day counterpart with statistical signficance above the 95% confidence level. (d–f) As per (a)–(c) but for anomalies of past-24-hr precipitation (fill) and precipitable water (contours). Contour interval is 1 mm with positive blue, negative dashed red, and zero omitted. [Colour figure can be viewed at wileyonlinelibrary.com]

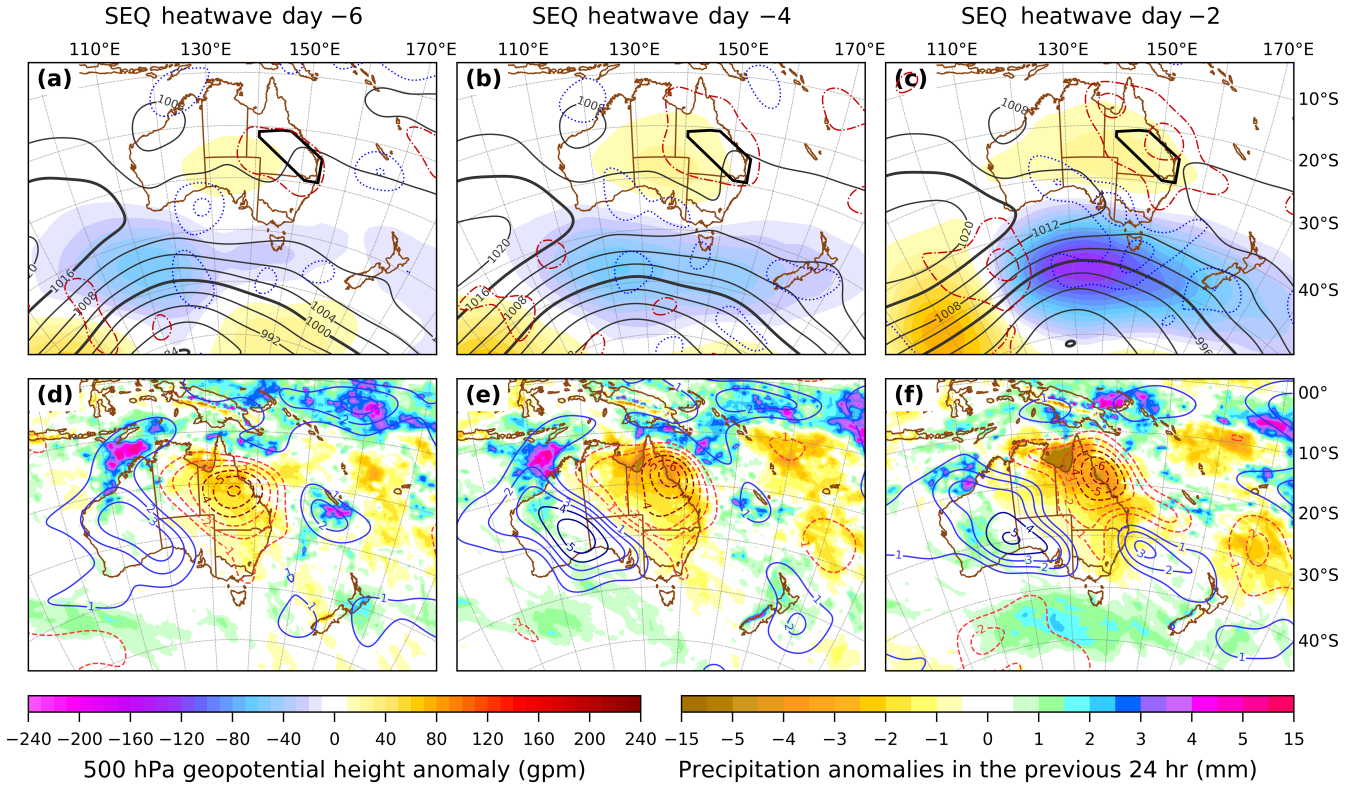

FIGURE 5 (a–c) Cluster 1, south and central eastern Queensland (SEQ) subdomain, regional heatwave day cases as per Figure 4(a), but instead for (a) day −6, (b) day −4, and (c) day −2. (d–f) Same, but as per Figure 4d. [Colour figure can be viewed at wileyonlinelibrary.com]

drier air (Figure 5d–f) and subsidence (Figure 5a–c) is evident throughout this lead-up and occurs on the downstream flank of the positive 500 hPa geopotential height anomaly as it migrates east and elongates zonally. Thus, the drier air preceding heatwaves can be at least partially attributed to mid-tropospheric subsidence ahead of the approaching upper ridge. Over the final few days prior to day 0, a positive moisture anomaly develops over southeastern Queensland, roughly co-located with the surface trough on the upstream flank of the upper ridge (Figures 4d and 5f). This is consistent with the result of Quinting *et al.* (2018), who noted the moistening of air parcels a few days prior to arrival in Brisbane heatwaves. They also showed that a substantial fraction of the heatwave near-surface air originates in the southern Coral Sea west of about 165°E several days beforehand. This air is warmed adiabatically as it is transported west and subsides towards southeastern Queensland (their figs. 1 and 2). Figures 4a and 5b,c show the broad-scale subsidence in this offshore region over the same time frame.

The 500 hPa geopotential height and mid-tropospheric omega anomaly structures in Figure 4a are consistent with equatorward Rossby wave refraction in the case of RHW days, as found by Risbey *et al.* (2017) in the lead-up to heatwaves for southeastern Queensland. This is not the case for the NHW days, where neither the 500 hPa geopotential height nor the omega anomalies extend north of 30°, and their sequence has a zonal orientation. The refracted Rossby wave train over eastern Australia on SEQ RHW days (Figure 4a) is similar to that during enhanced convection in the South Pacific convergence zone (van der Wiel *et al.*, 2015, schematic in fig. 13), and suggests that the same wave train may be responsible for both phenomena.

Hovmöller plots of 350 K PV, AWB and mid-tropospheric omega anomalies (Figure 6) show mainly slight differences at Australian longitudes. RHW days are preceded by an anticyclonic PV anomaly near 120°E to 150°E around day −5 to day −3. PV anomalies and vertical motions in the Australian midlatitudes are slightly stronger for NHW days, but AWB breaking frequency is above average near 180°E on RHW days. The composite upper trough that propagates eastward through the South Pacific in the lead-up to and following RHW days and a stationary upper trough east of South America are not present on NHW days, although their relevance to SEQ heatwaves is not clear. Similarly, the slightly higher incidence of blocking between 190°E and 210°E following RHW days can be related to the upstream AWB (Berrisford *et al.*, 2007). However, these longitudes have the highest climatological frequency of blocking (e.g., Tibaldi *et al.*, 1994, fig. 19c), with a 3-day blocking frequency

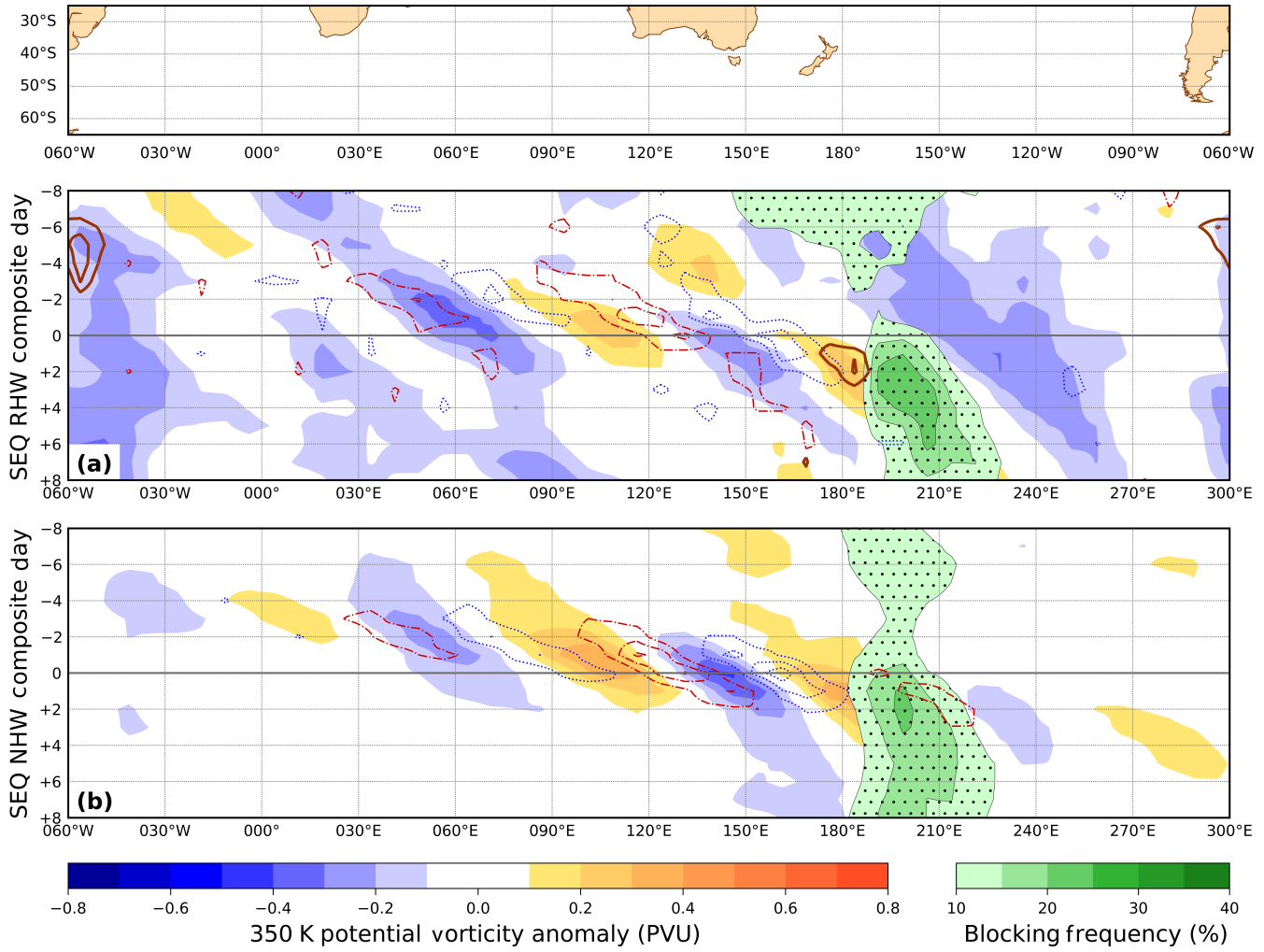

FIGURE 6 Composite of 350 K potential vorticity anomalies (fill), Tibaldi–Molteni blocking index (fill with contours and dot stippling), anticyclonic Rossby wave breaking (AWB; thick contours), and 400–600 hPa averaged omega vertical velocity anomalies (thin contours with red dash-dot positive, blue dotted negative, zero omitted) in Cluster 1, south and central eastern Queensland (SEQ) domain for (a) regional heatwave (RHW) days and (b) regional non-heatwave (NHW) days. Daily fields making up the composites are averaged over 7.5° longitude intervals, except Tibaldi–Molteni blocking index where the maximum value (0 or 1 at each grid point) is taken over the interval. AWB is divided by its December–March climatological value to emphasise wave breaking at longitudes near eastern Australia. AWB contours are multiples of the climatological frequency ≥2.0 at intervals of 0.5. Time is shown increasing downwards, with day 0 representing the composite dates of the RHW and NHW subsets. [Colour figure can be viewed at wileyonlinelibrary.com]

of just over 10% of all DJFM days. These results do not suggest that blocking (as a function of longitude only) is especially relevant to heatwaves in this Cluster 1 pattern.

4.2 | Cluster 4, VIC subdomain

The 500 hPa ridge in the south Tasman Sea (Figure 2d) lies further equatorward on RHW days and the trough upstream is stronger than for NHW days (Figure 7a,b). These results are statistically significant (Figure 7c), as is a slight reduction in 500 hPa geopotential height over northern Western Australia on RHW days that can be explained by strong latent heating above 500 hPa in tropical convection (Figure 7d). The composite surface pressure in the Tasman Sea is several hectopascals higher on RHW days, the upstream surface trough is deeper, and there is lower surface pressure between 50°S and 60°S from eastern Australian to New Zealand longitudes. The vertical motion anomalies in this wave train east of 120°E are also stronger on RHW days. All of these features indicate that the Rossby waves associated with RHW days are more amplified than those of NHW days, and have propagated further equatorward. Hovmöller charts of the RHW and NHW composite time series (Figure 8) confirm this first assessment. PV anomalies at 350 K in the Australian region have larger amplitude and are slower moving from day −4 to day +2 than those associated with NHW days.

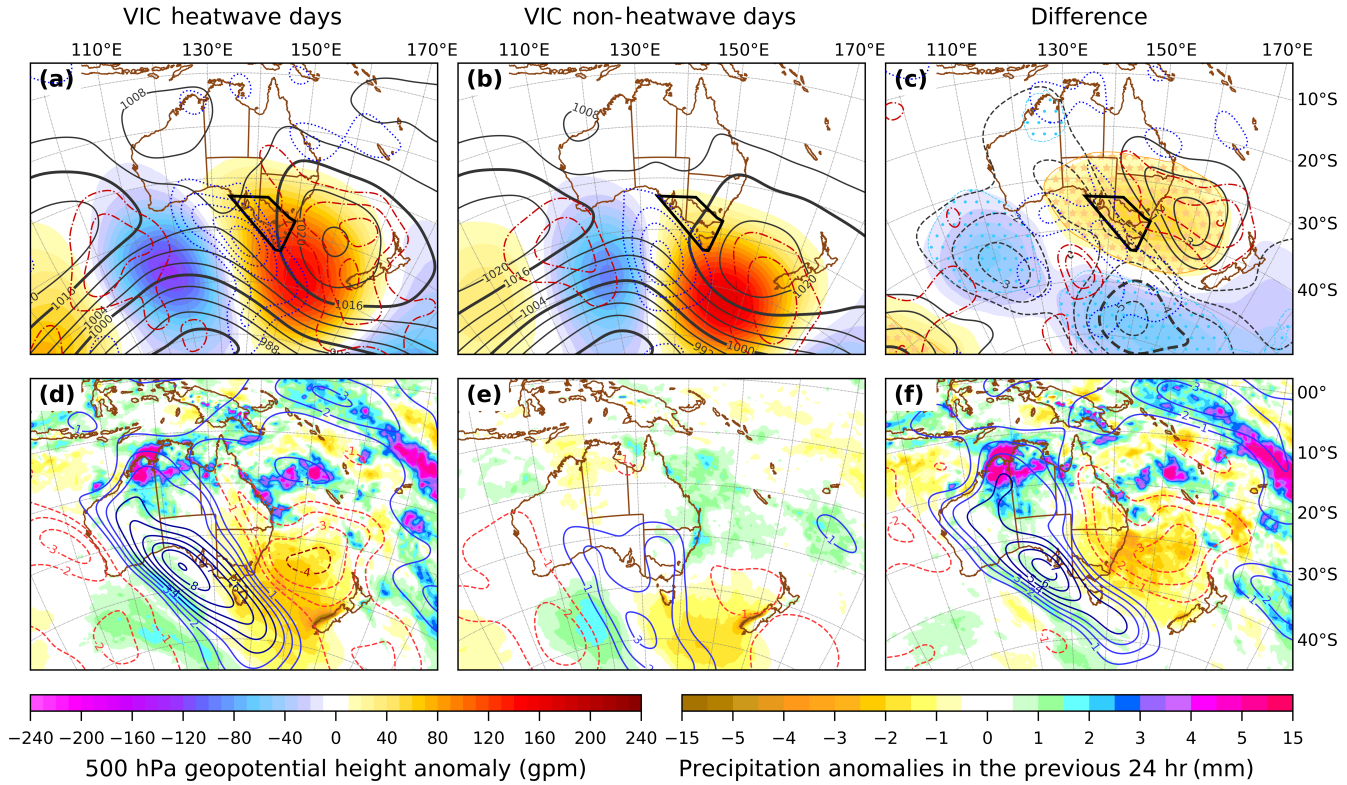

FIGURE 7 As per Figure 4, but for Cluster 4, Victoria, Tasmania, southeastern South Australia (VIC) subdomain. [Colour figure can be viewed at wileyonlinelibrary.com]

Enhanced convection occurs over tropical north and northwestern Australia on RHW days and is linked to a vast plume of moisture over western and central Australia that feeds into the poleward conveyor belt on the upstream flank of the upper ridge (Figure 7d). These anomalies are consistent also with the findings of Parker *et al.* (2013, 2014) and Quinting and Reeder (2017) for Victorian heatwaves. In contrast, NHW days are drier than usual over the northern Australian Tropics, and the moist anomaly upstream of the upper ridge is much weaker and confined to the midlatitudes (Figure 7e,f). In both cases the positive precipitable water anomaly is almost co-located with the band of ascending motion on the upstream flank of the upper ridge. However, the greater moisture and stronger ascent in this band on RHW days implies stronger and more extensive latent heating than on NHW days. Much of the air in the upper anticyclone on Victorian heatwave days is heated diabatically as it overtakes and ascends through this band over the final few days of its eastward journey (Quinting & Reeder, 2017, their figs. 6 and 7). The development of the poleward moist ascending flow over this time frame for RHW days is shown in Figure 9.

The more amplified moisture plume on RHW days may reduce the nocturnal long-wave cooling over the VIC subdomain. It is also, to some degree, a tracer for a poleward flow originating in the outflow from enhanced tropical convection over northwestern Australia. Upper tropospheric anticyclonic PV anomalies that arise in tropical convection can amplify the upper anticyclone in Victorian heatwaves by direct advection into the upper anticyclone, and through anticyclonic PV advection that perturbs the midlatitude waveguide (Parker *et al.*, 2013). These mechanisms are contributing factors in the AWB that characterises Victorian heatwaves (Parker *et al.*, 2014, fig. 2). The absence of these ingredients on NHW days explains the striking differences in the AWB frequency for RHW and NHW days in Figure 8. Following RHW days, AWB occurs with up to five-and-a-half times the climatological frequency near 150°E, but with no greater than the climatological frequency for NHW days. In some RHW cases it appears that two AWB events may occur, as there are AWB frequency maxima at day −3 and day +1. As with Cluster 1 (SEQ), blocking is not a distinguishing feature of RHW days. Although the onset of blocking following the large-scale AWB that occurs with RHW days is clear, its frequency between the Tasman Sea and 190°E is actually higher on NHW days.

Air over the Tasman Sea is also much drier on RHW days (Figure 7d–f) and, as with the Cluster 1 (SEQ) case, this is explained by mid-tropospheric subsidence over this region (Figure 7a). For NHW days this subsidence is considerably weaker and largely confined to the southeast Tasman Sea (Figure 7b). Quinting and Reeder (2017) showed that near-surface air in Victorian heatwaves is

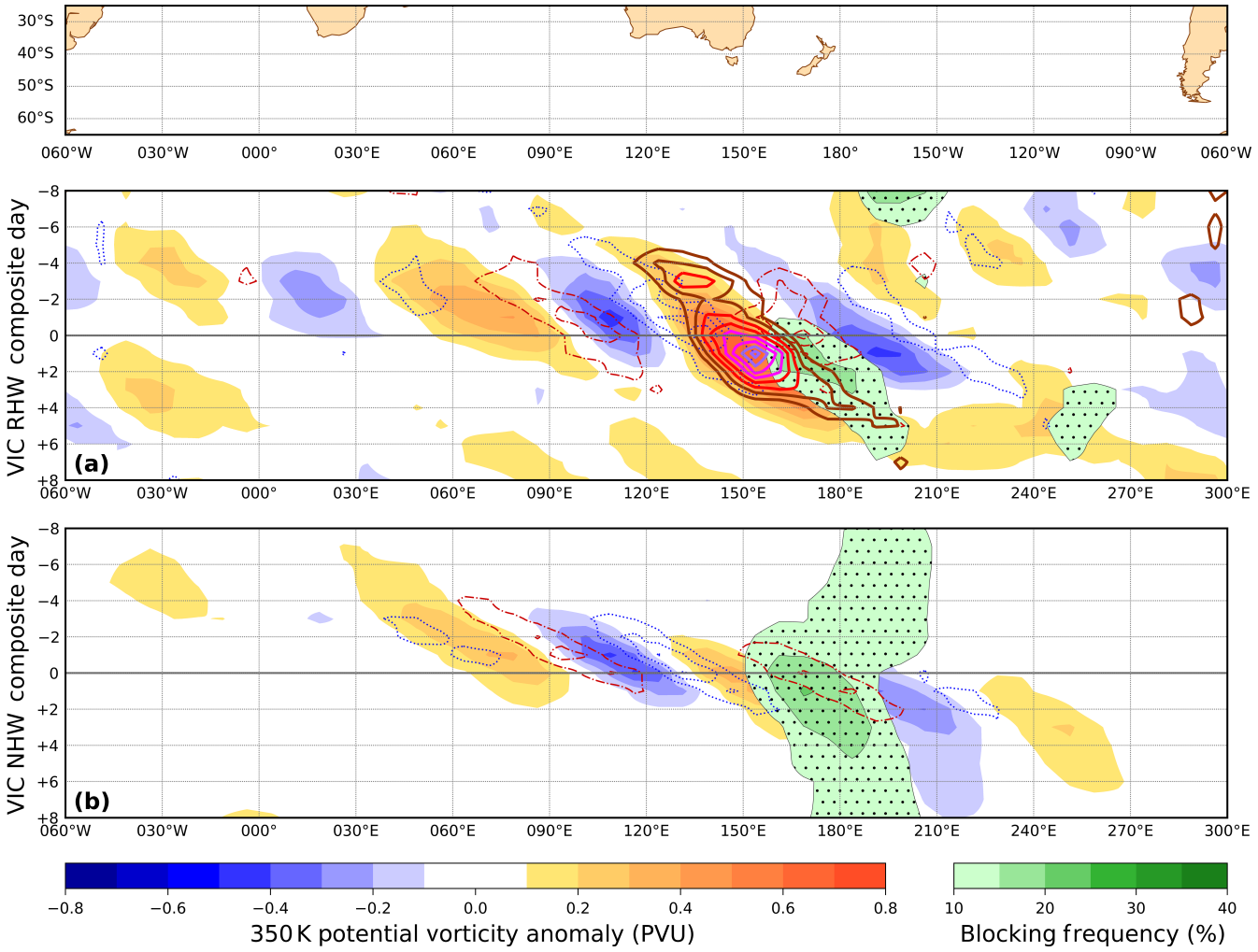

FIGURE 8 As per Figure 6, but for Cluster 4, Victoria, Tasmania, southeastern South Australia (VIC) subdomain. [Colour figure can be viewed at wileyonlinelibrary.com]

mostly situated in the lower troposphere over the Tasman Sea 3–6 days beforehand, and is warmed adiabatically over this period. Figure 9a–c shows subsidence over the Tasman Sea for several days prior to RHW days. The subsidence then strengthens as the upper anticyclone approaches and shifts into the northern Tasman Sea on day 0. This is a similar finding to Parker *et al.* (2014, their fig. 5), who showed that strengthening subsidence at 150°E ahead of the intensifying upper anticyclone shifts north of 40°S on day 1 of Victorian heatwaves. The Hovmöller plot for RHW days also shows near stationary subsidence at Tasman Sea longitudes from day −4 to day 0, which is a clear contrast to the propagating subsidence from day −2 to day 0 with NHW days.

4.3 | Cluster 5, SWQ subdomain

The results for this cluster are a hybrid of those for Cluster 1 (SEQ) and Cluster 4 (VIC). RHW days have a stronger 500 hPa ridge over central eastern Australia and a broader midlatitude 500 hPa trough that extends further west than NHW days (Figure 10a–c). The 500 hPa geopotential height fields show enhanced equatorward Rossby wave propagation on RHW days, similar to Cluster 1. The composite surface trough over the southwestern flank of the southwestern Queensland (SWQ) subdomain is also slightly deeper. The RHW day composite has lower surface pressure throughout the midlatitudes south of mainland Australia, especially south of Western Australia. Similar to with Cluster 1 (SEQ), there is enhanced baroclinicity on RHW days between 25°S and 45°S that is statistically significant at Australian longitudes (Figure 10c).

There are negative rainfall and precipitable water anomalies over Queensland on RHW days (Figure 10d), and a region of subsidence extends from southeastern Queensland across the northern and eastern Tasman Sea (Figure 10a). The link between tropical convection and the poleward transport of moisture over Australia on RHW days is similar to Cluster 4, although the precipitation anomalies lie 5°–10° further to the north. The

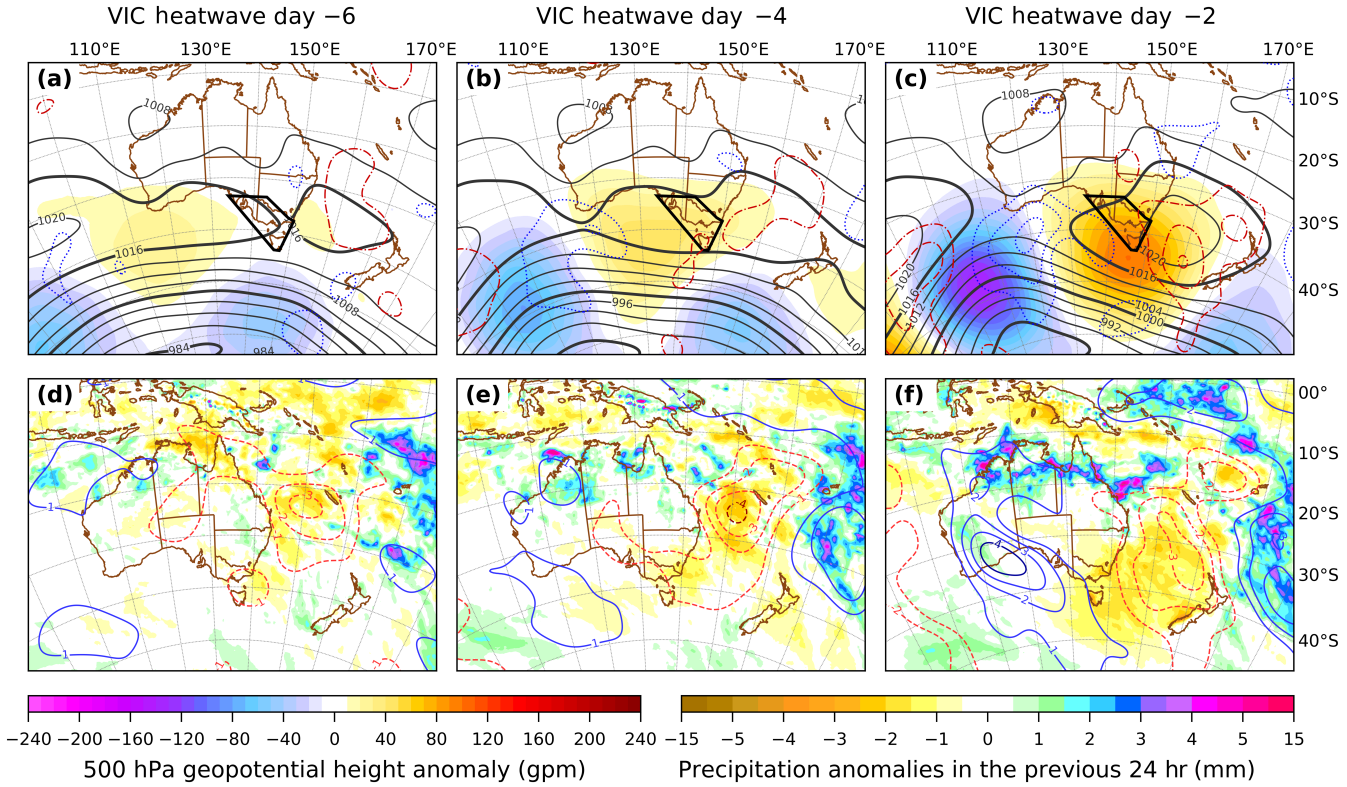

FIGURE 9 As per Figure 5, but for Cluster 4, Victoria, Tasmania, southeastern South Australia (VIC) subdomain. [Colour figure can be viewed at wileyonlinelibrary.com]

moist conveyor belt, which has a more zonal orientation, again coincides with a region of ascending air. Moisture anomalies are considerably stronger on RHW days than on NHW days (Figure 10d–f), presumably leading to enhanced latent heating as described for Cluster 4 (VIC).

From day −2 to day +2, the 350 K PV anomalies and associated mid-tropospheric vertical motions are similar for both RHW and NHW days west of 150°E (Figure 11). East of 150°E, AWB is enhanced at Tasman Sea longitudes for RHW days and the downstream trough is stronger than its NHW counterpart. The AWB frequency on RHW days exceeds that of Cluster 1 but is considerably lower than with Cluster 4. The propagation at Indian Ocean longitudes is slower on RHW days prior to day −2. After day +2, anticyclonic anomalies dominate the region from 60°E to 200°E, with further enhanced AWB near 170°E. Blocking frequency peaks near 190°E from day +2 to day +4 and is higher following NHW days.

4.4 | Cluster 7, NSW Australia subdomain

RHW days have stronger positive 500 hPa geopotential height anomalies over southeastern Australia than NHW days do (Figure 12a,b). Composite MSLP for RHW days shows a weak high-pressure cell in the Tasman Sea, but NHW days have a zonally oriented ridge south of mainland Australia. Surface pressure over southern and western Australia is lower on RHW days, especially Victoria and South Australia. These surface-pressure features indicate that heatwaves preferentially occur in the subset of days in this cluster with higher pressure over the Tasman Sea (rather than west of Bass Strait). Amplification of the Rossby wave train on RHW days is statistically significant (Figure 12c), but, unlike Cluster 4 (VIC), there is no statistically significant link with the pressure field over the Kimberley region of northeastern Western Australia.

Precipitable water anomalies are once again far stronger for RHW days than NHW days (Figure 12d–f). RHW days have enhanced precipitation over the Torres Strait and Coral Sea, similar to Cluster 4 (VIC) but shifted a few degrees northeast. On RHW days, a precipitable water maximum is again evident on the upstream flank of the upper ridge over western and central Australia, and extends over Victoria into the Tasman Sea. However, the air over Queensland and northeastern New South Wales is far drier. South of 25° these moist/dry anomalies are co-located with regions of ascent/subsidence (Figure 12a). The corresponding regions of ascent and subsidence on NHW days are situated several degrees further south. Moreover, they are less extensive, and in the case of the

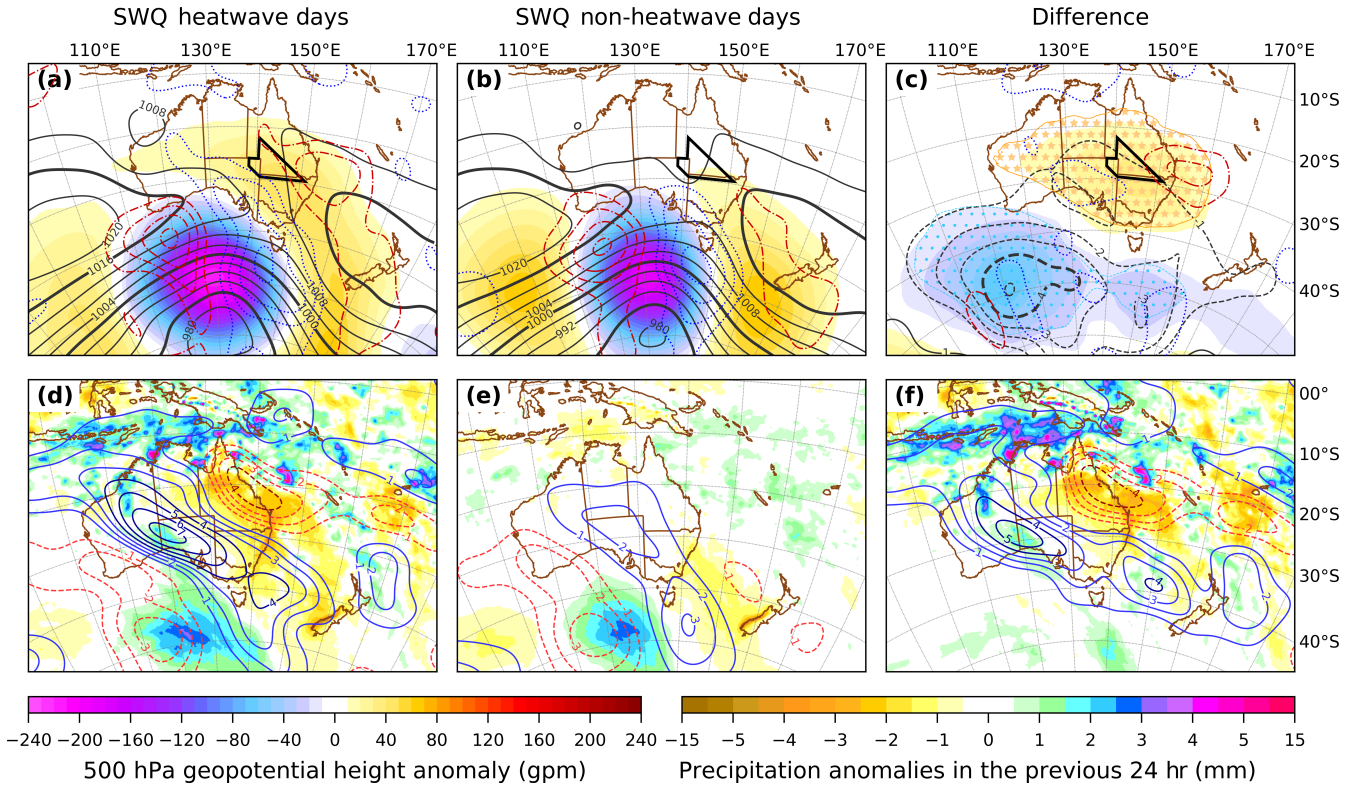

FIGURE 10 As per Figure 4, but for Cluster 5, southwestern Queensland (SWQ) subdomain. [Colour figure can be viewed at wileyonlinelibrary.com]

ascending anomaly are weaker than for RHW days. As with the other clusters, the overall picture for RHW days is one of stronger anomalies that have propagated further equatorward than those of NHW days.

The weak Rossby wave propagation signatures in the Hovmöller plots (Figure 13) are a result of weaker departures from climatology and a greater spread in the phase of this cluster. However, the peak AWB frequency on RHW days is second only to Cluster 4 (VIC). Aside from persistence, the most common 1-day precursor for this weakly amplified pattern is Cluster 2, and the highest MSLP in Cluster 2 occurs west of Bass Strait. For RHW days though, Clusters 5 and 4 with the highest surface pressure in the Tasman Sea are most common 1 day beforehand (excluding persistence). The weakly amplified state (Cluster 7) has the lowest incidence of downstream blocking of all the seven weather states out to day +4. Although strong AWB occurs prior to RHW days, it is followed by relaxation of the pattern on day 0.

A feature in common with Cluster 5 is the prevalence of anticyclonic PV anomalies from 120°E to 210°E following day 0, with subsequent wave-breaking around day +4. A similar finding of a quiescent period of weak anticyclonic anomalies a few days after the cessation of Victorian heatwave events was reported by (Parker *et al.*, 2014, their fig. 4a). Clusters 7 (31%) and 5 (25%) are most common on the final day of VIC RHW events, aside from Cluster 4 (34%). One day following their cessation, Clusters 7 (25%) and 5 (22%) are the most common. Further analysis of the Rossby wave packets associated with heatwaves is needed to fully explain this result, but it may indicate higher extended range predictability for episodes of summer weather that conclude with heatwaves south of 30°S in southeastern Australia.

In each of the four cluster subdomains examined, upper-tropospheric anticyclonic anomalies are found where RHW days occur most frequently. These are stronger for RHW days than NHW days and have larger positive precipitable water anomalies on their upstream flank. These overlap spatially with mid-tropospheric ascending motion anomalies on and prior to RHW days, implying enhanced latent heating in these regions. In all cases, statistically significant differences in the 500 hPa geopotential height fields show that the upper anticyclonic anomalies on RHW days have propagated further equatorward than on NHW days. The RHW anticyclonic anomalies are strong, with frequent AWB over Victoria, Tasmania, and South Australia, but weaken north and eastward through the Subtropics. Downstream of these anomalies, subsidence occurs over oceanic regions east of Australia on and prior to RHW days that previous studies have shown contributes to adiabatic compression of near-surface parcels in southeast Australian heatwaves (Parker *et al.*, 2019; Quinting *et al.*, 2018; Quinting &

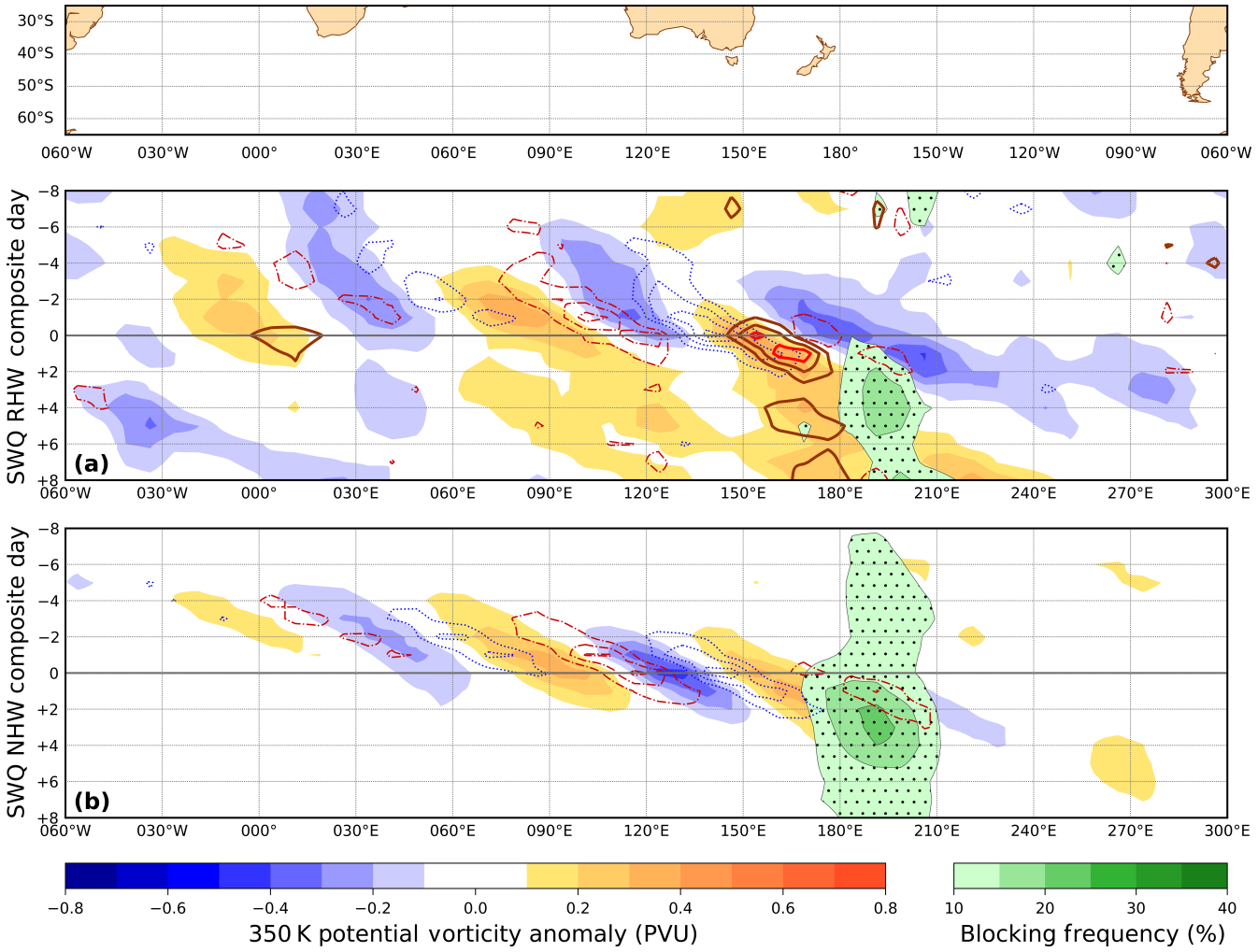

FIGURE 11 As per Figure 6, but for Cluster 5, southwestern Queensland (SWQ) subdomain. [Colour figure can be viewed at wileyonlinelibrary.com]

Reeder, 2017). Subsidence downstream of the corresponding anticyclones on NHW days is either weaker or confined to regions considerably further to the south.

5 | SENSITIVITY OF MAXIMUM TEMPERATURE

As similar weather patterns produce both RHW and NHW days, one might ask what aspects of those patterns most strongly influence surface temperature? Ensemble sensitivity analysis measures linear relationships between a forecast metric and a set (ensemble) of precursor forecasts or analyses (e.g., Ancell & Hakim, 2007; Parker *et al.*, 2018; Torn & Hakim, 2008). The presumption of a linear relationship between a forecast parameter and a parent field makes the results easy to interpret, but their validity may have limited lead-time for strongly nonlinear systems. The technique has been adapted to explore relationships between observed meteorological properties and their atmospheric predecessors (Dacre & Gray, 2013; Garcies & Homar, 2009). In this section, the sensitivities of DJFM 3-day-mean maximum temperature anomalies over the cluster subdomains in Section 3 (the metric) to several precursor fields are analysed for the ensemble of all days belonging to the corresponding cluster. The 3-day average (of days 0, +1, and +2) is used to ensure that the sensitivities are relevant for heatwaves, which have been defined as extreme heat events of at least 3 days in duration.

Using the same notation as Parker *et al.* (2018), the uncorrected sensitivity of an ensemble of precursor fields x^k to a set of observations J^k, where $k = 1, \ldots, K$, is the slope of a linear regression m_{ij} of the observations onto the ensemble at each point on a grid (i, j) for latitudes $i = 1, \ldots, M$ and longitudes $j = 1, \ldots, N$. Then:

$$m_{ij} = \left(\frac{\partial J}{\partial x}\right)_{ij} = \frac{\mathrm{Cov}\, J^k x_{ij}^k}{\mathrm{Var}\, x_{ij}^k}.$$

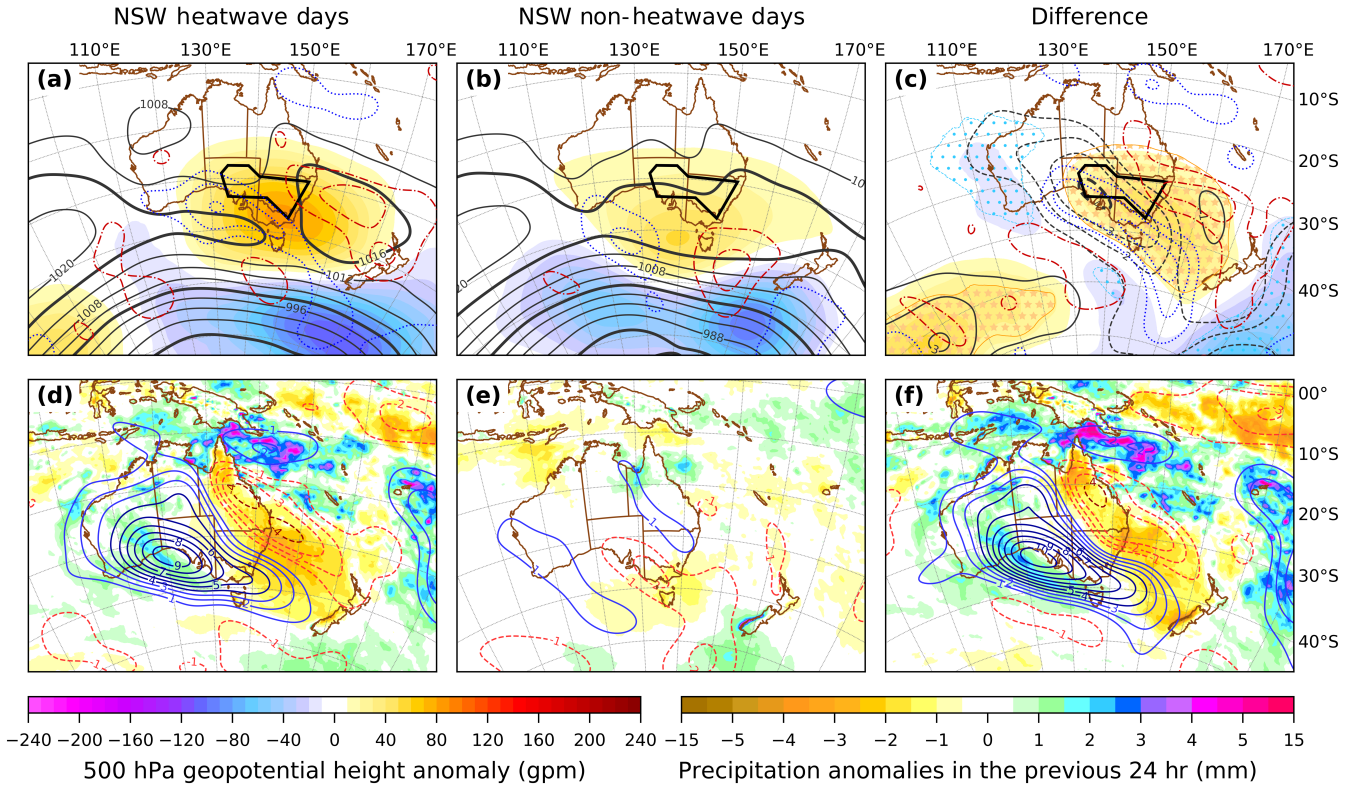

FIGURE 12 As per Figure 4, but for Cluster 7, inland New South Wales and eastern South Australia (NSW) subdomain. [Colour figure can be viewed at wileyonlinelibrary.com]

To avoid spuriously large sensitivities at points with tenuous linear relationships, a multiplicative correction factor α_{ij} is applied to dampen the sensitivities at grid points where the correlation coefficient r^2_{ij} is small. A threshold of $r^2_{\text{min}} = 0.1$ is used here. The correction factor is defined as

$$\alpha_{ij} = \begin{cases} 1 & \text{if } r^2_{ij} \geq r^2_{\text{min}} \\ r^2_{ij}/r^2_{\text{min}} & \text{if } r^2_{ij} < r^2_{\text{min}} \end{cases}.$$

Further multiplication by the standard deviation of the ensemble field σ_{ij} defines the final corrected senstivity S_{ij} in the same units as the observations, where

$$S_{ij} = m_{ij}\alpha_{ij}\sigma_{ij}. \quad (1)$$

Equation (1) can be interpreted as the linear response in the units of the metric to a one standard deviation change in the ensemble field. An area of positive/negative sensitivity to a particular meteorological field implies that increasing/decreasing the field value there (compared with the cluster mean) acts to increase 3-day-mean maximum temperature over the selected cluster subdomain. Sensitivities of 3-day-mean maximum temperature anomalies to anomalies of 500 hPa geopotential height, MSLP, and precipitable water[2] at 00 UTC on day 0, for the SEQ, VIC, SWQ, and NSW cluster subdomains, are shown in Figure 14. Rainfall anomalies were also tested but are not shown, as each cluster had negative sensitivity almost co-located with the subdomain tested. This correlation between lower rainfall and higher temperature was presumed to be strongly influenced by reduced cloudiness and soil moisture.

Positive 500 hPa geopotential height anomalies over northern Australia are associated with warmer weather over the SEQ subdomain in Cluster 1, and a similar relationship is evident in the MSLP anomalies (Figure 14a,b). Decreases in the pressure field on the eastern and western flanks of the negative anomalies south of Tasmania are also linked to higher 3-day-mean maximum temperature. This is consistent with SEQ RHW days occurring preferentially when the trough south of Tasmania is broader, and 500 hPa geopotential height is higher over northern Australia (Figure 4a–c). Weaker positive sensitivities are present over northern Australia up to 7 days earlier (not shown).

In contrast, non-stationary sensitivities to the pressure field for the VIC (Figure 14d,e) and SWQ (Figure 14g,h) subdomains in Clusters 4 and 5 respectively only become prominent 4 days earlier and intensify with the approaching Rossby wave. In both cases, a more amplified 500 hPa ridge and broader upstream trough are associated with

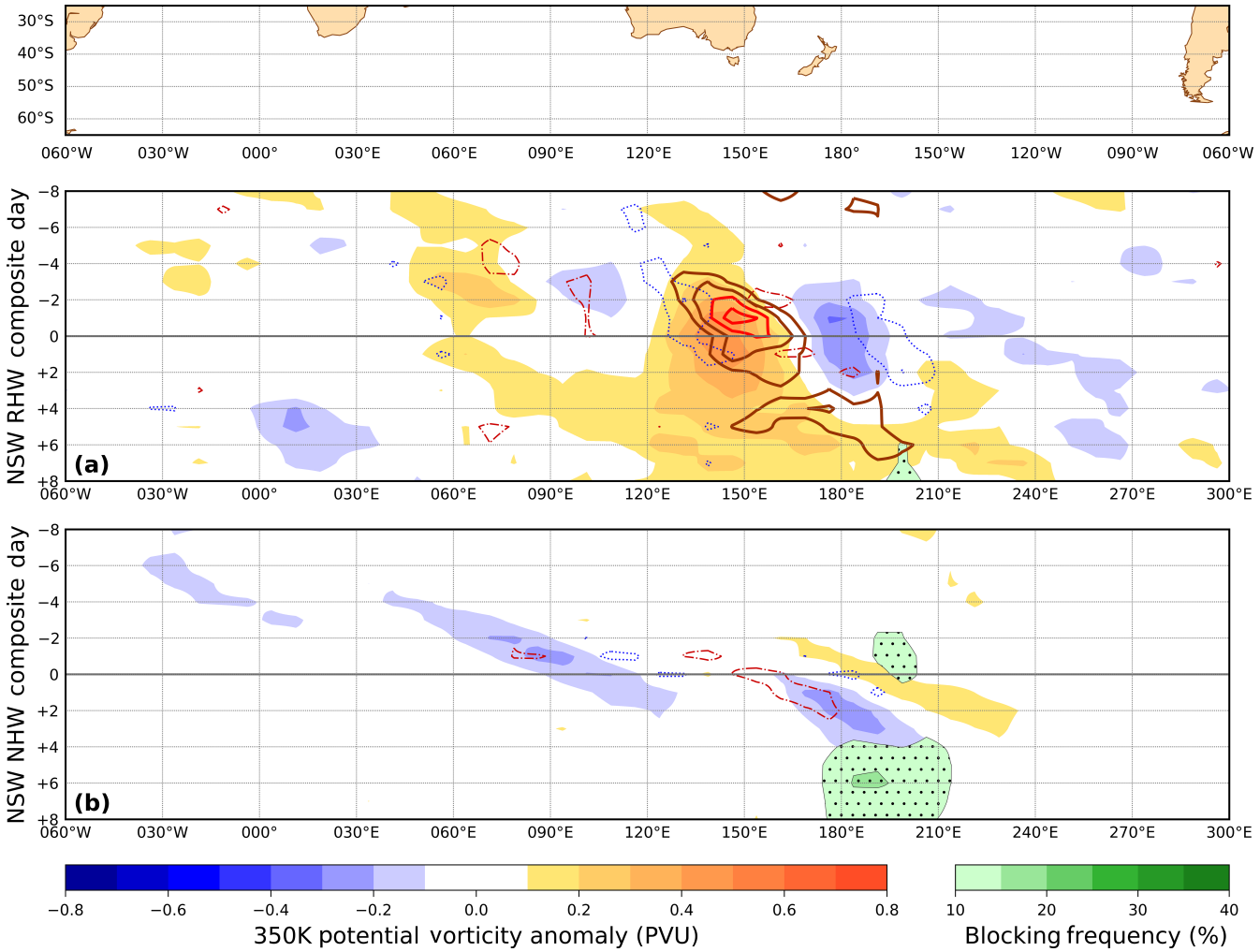

FIGURE 13 As per Figure 6, but for Cluster 7, inland New South Wales and eastern South Australia (NSW) subdomain. [Colour figure can be viewed at wileyonlinelibrary.com]

higher 3-day-mean maximum temperature, consistent with the composite RHW day signatures in those regions (Figures 7a–c and 10a–c). These sensitivities are stronger for the more southern VIC subdomain, which lies closer to the mean position of the midlatitude jet.

Sensitivity to the pressure field in the NSW subdomain, Cluster 7 (Figure 14j,k), also occurs in a negative/-positive couplet consistent with a propagating wave. The phase is very similar to the VIC subdomain results in Cluster 4, albeit shifted about 5° northward in latitude. Here, prolonged warm weather is favoured in the subset of cases where the upper ridge is stronger over southeastern Australia, similar to the composite result for RHW days (Figure 12a–c).

Sensitivity to precipitable water anomalies shows a marked variation with latitude. A drier troposphere over Queensland is associated with increased 3-day-mean maximum temperature in the SEQ subdomain of Cluster 1 and the SWQ subdomain of Cluster 5 (Figure 14c,i). This is very consistent with the average findings for RHW days in these regions (Figures 4d–f and 10d–f) where the drier air coincides with regions of broad-scale subsidence. In the case of the SEQ subdomain in Cluster 1, the negative sensitivity is still evident 7 days earlier. It is important to note that the sensitivity is not negative near and to the southeast of Brisbane. In this far southeastern corner of Queensland, precipitable water is higher than the cluster mean there on RHW days, although the nature of its contribution to the heatwave conditions has not yet been fully explained.

For the more southern subdomains of VIC in Cluster 4 and NSW in Cluster 7, sensitivity to precipitable water is weaker and tied to the propagating wave (Figure 14f,l). Conditions are warmer when there is increased column moisture on the upstream flank of the upper ridge and less moisture on the downstream flank, a pattern that is consistent with the corresponding RHW day composites (Figures 7d–f and 12d–f). It is mostly the case that dry and subsiding air is located near regions of negative

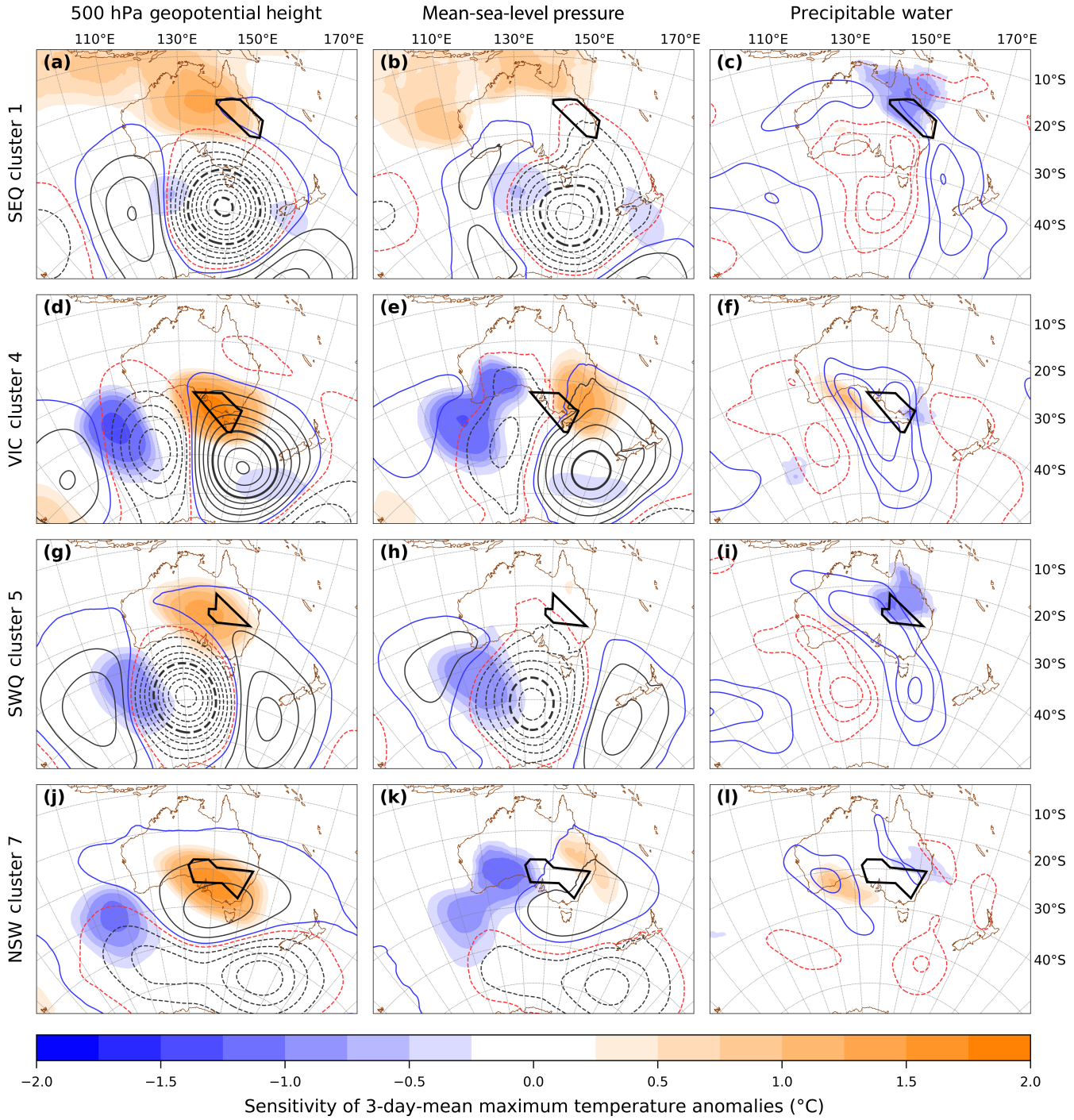

FIGURE 14 Sensitivity of 3-day-mean maximum temperature anomalies (fill) to anomalies of (a, d, g, j) 500 hPa geopotential height, (b, e, h, k) mean-sea-level pressure (MSLP), and (c, f, i, l) precipitable water on day 0. For subdomains (black polygons) (a–c) south and central eastern Queensland (SEQ) in Cluster 1, (d–f) Victoria, Tasmania, southeastern South Australia (VIC) in Cluster 4, (g–i) southwestern Queensland (SWQ) in Cluster 5, and (j–l) inland New South Wales and eastern South Australia (NSW) in Cluster 7. Contours (zero omitted) are cluster-mean anomalies: 500 hPa geopotential height, black every 20 gpm with negative dashed, ±100 gpm bold, +5 gpm blue, −5 gpm red; MSLP, black every 2 hPa, negative dashed, ±10 hPa bold, +1 hPa blue, −1 hPa red; precipitable water every 1 mm with blue positive and red dashed negative. [Colour figure can be viewed at wileyonlinelibrary.com]

sensitivity, which is consistent with adiabatic warming; likewise, moist, ascending air is situated near regions of positive sensitivity, implying latent heating. One exception is the negative sensitivity over Victoria between 145°E and 148°E, a region that has positive moisture anomalies on RHW days. The reasons for this are not fully clear but may

be related to cloudiness and rainfall forced by upslope flow over this mountainous region in cases where the hottest conditions are further west in the subdomain. Negative sensitivity to rainfall in this cluster (not shown) is largest in this area and supports this idea.

For the VIC subdomain, no sensitivity to precipitable water is observed prior to day +1. The more northern NSW subdomain, however, has aspects of the lower latitude SEQ and SWQ examples. Here, the negative sensitivity is evident back to day +4 and is strongest/most extensive at day +2 near northeastern South Australia (not shown). It is also possible that enhanced moisture over the VIC and NSW subdomains may limit nocturnal long wave surface cooling on RHW days. However, this possibility does not appear to greatly influence the daytime maximum temperature as the sensitivity to precipitable water is not positive in these subdomains.

6 | CONCLUSIONS

A synoptic climatology of the southeastern Australian extended summer (DJFM) was constructed by *k*-means cluster analysis of 500 hPa geopotential height anomalies over a domain centred on southeastern Australia, to compare heatwave days in this region against non-heatwave days with a similar weather pattern.

Four of the seven weather states in this climatology have geographically distinct regions with a high grid-point frequency of heatwave days that together cover most of southeastern Australia. Around 8% of days in these clusters satisfies a grid-point heatwave definition over 10% or more of the area of these preferred heatwave subdomains—an event that was referred to as an RHW day. In each case, an upper ridge is situated over the subdomain on these RHW days that is stronger than on NHW days. Sensitivity analysis of 3-day-mean maximum temperature anomalies in these regions shows positive correlations with the strength of the upper ridge.

South of 30°S, heatwaves are favoured in weather states with a surface high-pressure system in the Tasman Sea. The highest frequency of grid-point heatwave days lies over VIC when the flow is strongly amplified (Cluster 4) and over NSW when the flow is weakly amplified (Cluster 7). Compared with non-heatwave days, RHW days have higher pressure in the Tasman Sea and lower surface pressure over South Australia and enhanced precipitation over the Coral Sea and Australian Tropics. The composite AWB frequency near 150°E is up to five-and-a-half times the climatological average on RHW days, but no higher than average on NHW days.

North of 30°S, the grid-point heatwave-day frequency is highest when a midlatitude trough south of eastern Australia extends over parts of New South Wales and Queensland, with higher surface temperature on its northeastern flank. This trough has a broader longitudinal extent for RHW days. The frequency of AWB at these latitudes is greatly reduced, with little difference between RHW and NHW days. This result agrees with earlier findings for Brisbane heatwaves that showed only a minor undulation of the dynamic tropopause at 350 K (Quinting *et al.*, 2018, fig. 4). RHW days have lower surface pressure over southeastern Australia than NHW days do, and less precipitation over Queensland.

In all four cases analysed, the pressure, moisture, and vertical motion anomalies on RHW days are consistent with Rossby wave propagation that is more equatorward than for NHW days in the same cluster. Mid-tropospheric subsidence was found downstream of the upper ridge over the Tasman and Coral seas on and before RHW days, consistent with findings of recent studies for southeastern Australia that show these are regions where a large proportion of near-surface heatwave air parcels are warmed adiabatically a few days beforehand (Parker *et al.*, 2019; Quinting *et al.*, 2018; Quinting & Reeder, 2017). The dry anomalies over much of Queensland that precede and accompany RHW days north of 27°S, and the negative correlation between precipitable water and 3-day-mean maximum temperature anomalies over southern Queensland, are well explained by these subsidence patterns. These latter results complement those of Gibson *et al.* (2017), who found that the likelihood of heatwaves increases over much of eastern Australia under conditions of low soil moisture for MSLP patterns that are similar to Clusters 1 and 5.

The positive precipitable water anomalies upstream of the upper ridge are considerably stronger for RHW days and they coincide with regions of ascent. The corresponding moisture anomalies for NHW days are much weaker and do not have a clear link to the Australian Tropics, which are drier. Moreover, the associated regions of ascent are both weaker and located further poleward on NHW days. These features of the moisture and vertical motion fields suggest enhanced latent heating of air parcels in these poleward conveyor belts on RHW days, consistent with the findings of Quinting and Reeder (2017), who showed that much of the upper anticyclone air in Victorian heatwaves has undergone this process as it ascends from the west.

Blocking, at least as a function of longitude only, is not found to distinguish heatwaves from other days with a similar synoptic-scale weather pattern, as it generally occurs more often with non-heatwave days (southeastern Queensland excepted). However, the several days of weak anticyclonic anomalies that follow heatwave days in Clusters 5 and 7 is distinctive and may be important for their forecastability.

The key finding of this study is that the more equatorward and amplified Rossby wave propagation on heatwave days is a major factor in setting up the regional distribution of moisture and vertical motions that are known to be important for adiabatic warming and latent heating of heatwave air parcels in southeastern Australia. These ingredients are largely missing or displaced significantly further poleward on non-heatwave days. More work could be undertaken to determine how greatly the thermodynamic and circulatory trajectories of non-heatwave days differ from those of heatwave days with a similar synoptic pattern to test this hypothesis further.

ACKNOWLEDGEMENTS

We gratefully acknowledge the Australian Research Council Centre of Excellence for Climate Extremes (CE170100023) for funding this research, the National Computing Infrastructure and ECMWF for making available the ERA5 dataset, and the Bureau of Meteorology for the AWAP dataset. We thank the Bureau of Meteorology Training Centre and Karlsruhe Institute of Technology for time provided to CRH and JFQ. The contribution of JFQ was partly funded by the Helmholtz Association as part of the Young Investigator Group "Sub-seasonal Predictability: Understanding the Role of Diabatic Outflow" (SPREADOUT, grant VH-NG-1243). CRH would like to thank Robert Leighton (Bureau of Meteorology, now retired) for several instructive conversations on Melbourne heatwaves. Finally, we would like to thank two anonymous reviewers. Their thorough and very helpful considerations greatly improved this article.

DATA AVAILABILITY STATEMENT

Gridded datasets from the Australian Water Availability Project and the ERA5 are available from the Australian National Computing Infrastructure (NCI Australia). Derived data supporting the findings of this study are available from the corresponding author CRH on request.

The ERA5 data that support the findings of this study are available from the ECMWF. Restrictions apply to the availability of these data, which were used under license for this study. Data was obtained from https://nci.org.au/ with the permission of ECMWF. The AWAP data that support the findings of this study are available from the Australian Bureau of Meteorology. Restrictions apply to the availability of these data, which were used under license for this study. Data were obtained from https://nci.org.au/ with the permission of Australian Bureau of Meteorology.

ENDNOTES

[1]Measurements from the Melbourne Regional Office site, which closed on January 6, 2015.

[2]Precipitable water sensitivity and anomaly fields are smoothed with spherical harmonics at $m = n = 36$.

ORCID

Cameron R. Henderson https://orcid.org/0009-0001-3109-6100

Julian F. Quinting https://orcid.org/0000-0002-8409-2541

REFERENCES

Ancell, B. & Hakim, G.J. (2007) Comparing adjoint- and ensemble-sensitivity analysis with applications to observation targeting. *Monthly Weather Review*, 135, 4117–4134.

Barriopedro, D., Fischer, E.M., Luterbacher, J., Trigo, R.M. & García-Herrera, R. (2011) The hot summer of 2010: Redrawing the temperature record map of Europe. *Science*, 332, 220–224.

Berrisford, P., Hoskins, B.J. & Tyrlis, E. (2007) Blocking and Rossby Wave Breaking on the Dynamical Tropopause in the Southern Hemisphere. *Journal of the Atmospheric Sciences*, 64, 2881–2898.

Black, E., Blackburn, M., Harrison, G., Hoskins, B. & Methven, J. (2004) Factors contributing to the summer 2003 European heatwave. *Weather*, 59, 217–223.

Coates, L., Haynes, K., O'Brien, J., McAneney, J. & de Oliveira, F.D. (2014) Exploring 167 years of vulnerability: An examination of extreme heat events in Australia 1844-2010. *Environmental Science & Policy*, 42, 33–44.

Coates, L., van Leeuwen, J., Browning, S., Gissing, A., Bratchell, J. & Avci, A. (2022) Heatwave fatalities in Australia, 2001–2018: An analysis of coronial records. *International Journal of Disaster Risk Reduction*, 67, 102671. Available from: https://www.sciencedirect.com/science/article/pii/S2212420921006324

Dacre, H.F. & Gray, S.L. (2013) Quantifying the climatological relationship between extratropical cyclone intensity and atmospheric precursors. *Geophysical Research Letters*, 40, 2322–2327.

Engel, C.B., Lane, T.P., Reeder, M.J. & Rezny, M. (2013) The meteorology of Black Saturday. *Quarterly Journal of the Royal Meteorological Society*, 139, 585–599.

Galarneau, T.J., Hamill, T.M., Dole, R.M. & Perlwitz, J. (2012) A multiscale analysis of the extreme weather events over Western Russia and Northern Pakistan during July 2010. *Monthly Weather Review*, 140, 1639–1664.

Garcies, L. & Homar, V. (2009) Ensemble sensitivities of the real atmosphere: Application to Mediterranean intense cyclones. *Tellus*, 61A, 394–406.

Gibson, P.B., Pitman, A.J., Lorenz, R. & Perkins-Kirkpatrick, S.E. (2017) The role of circulation and land surface conditions in current and future Australian heat waves. *Journal of Climate*, 30, 9933–9948.

Hartigan, J.A. & Wong, M.A. (1979) Algorithm AS 136: A K-means clustering algorithm. *Applied Statistics*, 28, 100–108.

Hersbach, H., Bell, B., Berrisford, P., Hirahara, S., Horányi, A., noz Sabater, J.M. et al. (2020) The ERA5 global reanalysis. *Quarterly Journal of the Royal Meteorological Society*, 146, 1999–2049.

Hoskins, B.J. & Ambrizzi, T. (1993) Rossby wave propagation on a realistic longitudinally varying flow. *Journal of the Atmospheric Sciences*, 50, 1661–1671.

IPCC. (2007) *Climate Change 2007: Synthesis Report. Contribution of Working Groups I, II and III to the Fourth Assessment Report of the*

Intergovernmental Panel on Climate Change. Tech. rep. Geneva, Switzerland: IPCC, p. 104.

Jones, D.A., Wang, W. & Fawcett, R. (2009) High-quality spatial climate data-sets for Australia. *Australian Meteorological and Oceanographic Journal*, 58, 233–248.

Leslie, L.M. (1980) Numerical modeling of the summer heat low over Australia. *Journal of Applied Meteorology*, 19, 381–387.

Matsueda, M. (2011) Predictability of Euro-Russian blocking in summer of 2010. *Geophysical Research Letters*, 38, 1–6.

Nairn, J.R., Fawcett, R. & Ray, D. (2009) *Defining and Predicting Excessive Heat Events: A National System*. Tech. Rep. 17. Melbourne: The Centre for Australian Weather and Climate Research, pp. 83–86.

National Climate Centre. (2009) *The Exceptional January-February 2009 Heatwave in South-Eastern Australia*. Tech. Rep. 17. Melbourne: Bureau of Meteorology, p. 11.

Ndarana, T. & Waugh, D.W. (2011) A climatology of Rossby wave breaking on the Southern Hemisphere tropopause. *Journal of the Atmospheric Sciences*, 68, 798–811.

O'Brien, L. & Reeder, M.J. (2017) Southern hemisphere summertime Rossby waves and weather in the Australian region. *Quarterly Journal of the Royal Meteorological Society*, 143, 2374–2388.

Parker, T., Woollings, T. & Weisheimer, A. (2018) Ensemble sensitivity analysis of Greenland blocking in medium-range forecasts. *Quarterly Journal of the Royal Meteorological Society*, 144, 2358–2379.

Parker, T.J., Berry, G.J. & Reeder, M.J. (2013) The influence of tropical cyclones on heat waves in Southeastern Australia. *Geophysical Research Letters*, 40, 6264–6270.

Parker, T.J., Berry, G.J. & Reeder, M.J. (2014) The structure and evolution of heat waves in Southeastern Australia. *Journal of Climate*, 27, 5768–5785.

Parker, T.J., Quinting, J.F. & Reeder, M.J. (2019) The synoptic-dynamics of summertime heat waves in the Sydney Area (Australia). *Journal of Southern Hemisphere Earth Systems Science*, 69, 116-130. https://doi.org/10.1071/ES19004

Perkins, S.E. & Alexander, L.V. (2013) On the measurement of heat waves. *Journal of Climate*, 26, 4500–4517.

Peters, D. & Waugh, D.W. (1996) Influence of barotropic shear on the poleward advection of upper-tropospheric air. *Journal of the Atmospheric Sciences*, 53, 3013–3031.

Pezza, A.B., van Rensch, P. & Cai, W. (2012) Severe heat waves in Southern Australia: Synoptic climatology and large scale connections. *Climate Dynamics*, 38, 209–224.

Pfahl, S. & Wernli, H. (2012) Quantifying the relevance of atmospheric blocking for co-located temperature extremes in the Northern Hemisphere on (sub-)daily time scales. *Geophysical Research Letters*, 39(12), L12807. https://doi.org/10.1029/2012GL052261

Purich, A., Cowan, T., Cai, W., van Rensch, P., Uotila, P., Pezza, A. et al. (2014) Atmospheric and oceanic conditions associated with Southern Australian heat waves: A CMIP5 analysis. *Journal of Climate*, 27, 7807–7829.

Quinting, J.F., Parker, T.J. & Reeder, M.J. (2018) Two synoptic routes to subtropical heat waves as illustrated in the Brisbane region of Australia. *Geophysical Research Letters*, 10, 700–708.

Quinting, J.F. & Reeder, M.J. (2017) Southeastern Australian heat waves from a trajectory viewpoint. *Monthly Weather Review*, 145, 4109–4125.

Reeder, M.J. & Smith, R.K. (1987) A study of frontal dynamics with application to the australian summertime "Cool Change". *Journal of the Atmospheric Sciences*, 44, 687–705.

Reeder, M.J., Spengler, T. & Musgrave, R. (2015) Rossby waves, extreme fronts, and wildfires in southeastern Australia. *Geophysical Research Letters*, 42, 2015–2023.

Risbey, J.S., O'Kane, T.J., Monselesan, D.P., Franzke, C.L.E. & Horenko, I. (2017) On the dynamics of austral heat waves. *Journal of Geophysical Research: Atmospheres*, 123, 38–57.

Robine, J.-M., Cheung, S.L.K., Le Roy, S., Van Oyen, H., Griffiths, C., Michel, J.-P. et al. (2008) Death toll exceeded 70,000 in Europe during the summer of 2003. *Comptes Rendus Biologies*, 331, 171–178.

Rossow, W.B., Tselioudis, G., Polak, A. & Jakob, C. (2005) Tropical climate described as a distribution of weather states indicated by distinct mesoscale cloud property mixtures. *Geophysical Research Letters*, 32, 1–4.

Röthlisberger, M. & Papritz, L. (2023) Quantifying the physical processes leading to atmospheric hot extremes at the global scale. *Nature Geoscience*, 16, 210–216.

Schalge, B., Blender, R. and Fraedrich, K. (2011) Blocking detection based on synoptic filters. *Advances in Meteorology*, 2011, 717812.

Schumacher, D.L., Hauser, M. & Seneviratne, S.I. (2022) Drivers and mechanisms of the 2021 pacific northwest heatwave. *Earth's Future*, 10(12), e2022EF002967. https://doi.org/10.1029/2022EF002967

Song, J., Li, C., Pan, J. & Zhou, W. (2011) Climatology of anticyclonic and cyclonic Rossby wave breaking on the dynamical tropopause in the southern hemisphere. *Journal of Climate*, 24, 1239–1251.

Takaya, K. & Nakamura, H. (2001) A formulation of a phase-independent wave-activity flus for stationary and migratory quasigeostrophic eddies on a zonally varying basic flow. *Journal of the Atmospheric Sciences*, 58, 608–627.

Thorncroft, C.D., Hoskins, B.J. & McIntyre, M.E. (1993) Two paradigms of baroclinic-wave life-cycle behaviour. *Quarterly Journal of the Royal Meteorological Society*, 119, 17–55.

Tibaldi, S., Tosi, E., Navarra, A. & Pedulli, L. (1994) Northern and Southern Hemisphere seasonal variability of blocking frequency and predictability. *Monthly Weather Review*, 122, 1971–2003.

Torn, R.D. & Hakim, G.J. (2008) Ensemble-based sensitivity analysis. *Monthly Weather Review*, 136, 663–677.

Trenberth, K.E. (1985) Persistence of daily geopotential heights over the Southern Hemisphere. *Monthly Weather Review*, 113, 38–53.

van der Wiel, K., Matthews, A.J., Stevens, D.P. & Joshi, M.M. (2015) A dynamical framework for the origin of the diagonal South Pacific and South Atlantic Convergence Zones. *Quarterly Journal of the Royal Meteorological Society*, 141, 1997–2010.

Wilks, D.S. (2006) *Statistical Methods in the Atmospheric Sciences*. International Geophysics Series, Vol. 91, 2nd edition. Burlington, MA, USA: Academic Press.

How to cite this article: Henderson, C.R., Reeder, M.J., Parker, T.J., Quinting, J.F. & Jakob, C. (2024) Summer Heatwaves in Southeastern Australia. *Quarterly Journal of the Royal Meteorological Society*, 1–21. Available from: https://doi.org/10.1002/qj.4816